clustering, current seismicity rates, and the rate of $M \geq 6$ events after the first year (Fig. 2D). Among sequences sampled that were consistent with New Madrid early clustering behavior and current seismicity rates, the mean number of $M \geq 6$ earthquakes from 1 year to 200 years post-mainshock was 135. At best, at some points in ETAS phase space ~1.7% of the sequences are consistent with our criteria. Results using a stricter criteria that includes the observation that no $M \geq 6$ earthquakes occurred in the region in the past 100 years (table S1) show that we can reject the long-lived aftershock hypothesis at even higher confidence.

Based on our statistical analysis, the hypothesis that current seismicity in the New Madrid region is primarily composed of aftershocks from the 1811–1812 sequence fails. This is because a sequence active enough at late times to produce the seismicity rates observed today and active enough at early times to produce the short-term clustering observed in the first few months would be highly likely to produce too many aftershocks in the intermediate times. If current seismicity in the New Madrid region is not composed predominantly of aftershocks, there must be continuing strain accrual. This is in agreement with recent work finding nonzero strain measurements in the region that are consistent with ongoing interseismic slip of about 4 mm/year (*21*), in contrast to earlier studies [e.g., (*22*)]. The spatial distribution of the stress pattern driven by this model would be generally consistent with the stress change caused by an earthquake on the Reelfoot fault. This could explain how ongoing microseismicity is not part of an aftershock sequence but is still consistent with the predicted stress change associated with the 1811–1812 sequence (*23*). If ongoing microseismicity does result from ongoing strain accrual, this suggests that the region, along with the neighboring Wabash Valley where nonzero strain has also been observed (*24*), will continue to be a source of hazard.

References and Notes

1. H. K. Gupta, N. P. Rao, B. K. Rastogi, D. Sarkar, *Science* **291**, 2101–2102 (2001).
2. S. E. Hough, M. Page, *J. Geophys. Res.* **116**, (B3), B03311 (2011).
3. A. C. Johnston, *Geophys. J. Int.* **126**, 314–344 (1996).
4. O. W. Nuttli, *Bull. Seismol. Soc. Am.* **63**, 227 (1973).
5. S. E. Hough, *Seismol. Res. Lett.* **80**, 1045–1053 (2009).
6. J. E. Ebel, K.-P. Bonjer, M. C. Oncescu, *Seismol. Res. Lett.* **71**, 283–294 (2000).
7. S. Stein, M. Liu, *Nature* **462**, 87–89 (2009).
8. F. Omori, *J. Coll. Sci. Imp. Univ. Tokyo* **7**, 111 (1895).
9. T. Utsu, *Geophys. Mag.* **30**, 521 (1961).
10. T. Utsu, Y. Ogata, R. S. Matsu'ura, *J. Phys. Earth* **43**, 1–33 (1995).
11. Y. Ogata, *J. Am. Stat. Assoc.* **83**, 9–27 (1988).
12. K. R. Felzer, R. E. Abercrombie, G. Ekstršm, *Bull. Seismol. Soc. Am.* **94**, 88–98 (2004).
13. Y. Ogata, *J. Geophys. Res.* **97**, (B13), 19845 (1992).
14. M. C. Gerstenberger, D. A. Rhoades, *Pure Appl. Geophys.* **167**, 877–892 (2010).
15. Y. Ogata, J. Zhuang, *Tectonophysics* **413**, 13–23 (2006).
16. A. L. Llenos, J. J. McGuire, Y. Ogata, *Earth Planet. Sci. Lett.* **281**, 59–69 (2009).
17. W. H. Bakun, M. G. Hopper, *Bull. Seismol. Soc. Am.* **94**, 64–75 (2004).
18. M. P. Tuttle, *Bull. Seismol. Soc. Am.* **92**, 2080–2089 (2002).
19. K. J. Coppersmith *et al*., Central and Eastern United States Seismic Source Characterization for Nuclear Facilities Project, Technical Report (Electric Power Research Institute, Palo Alto, CA, 2012).
20. S. E. Hough, *Bull. Seismol. Soc. Am.* **103**, 2767 (2013).
21. A. Frankel, R. Smalley, J. Paul, *Bull. Seismol. Soc. Am.* **102**, 479–489 (2012).
22. E. Calais, J. Y. Han, C. DeMets, J. M. Nocquet, *J. Geophys. Res.* **111**, (B6), 6402 (2006).
23. K. Mueller, S. E. Hough, R. Bilham, *Nature* **429**, 284–288 (2004).
24. G. A. Galgana, M. W. Hamburger, *Seismol. Res. Lett.* **81**, 699–714 (2010).
25. K. R. Felzer, R. E. Abercrombie, G. Ekström, *Bull. Seismol. Soc. Am.* **93**, 1433–1448 (2003).

Acknowledgments: We thank J. Hardebeck, C. Mueller, and two anonymous reviewers for comments on the manuscript. The CEUS-SSC catalog is available at: www.ceus-ssc.com/Report/Downloads.html. Author Contributions: M.T.P. did the ETAS modeling, and S.E.H. provided expertise on the historical catalog. Both authors participated in the writing.

Supplementary Materials

www.sciencemag.org/content/343/6172/762/suppl/DC1
Materials and Methods
Fig. S1
Table S1
References (*26*–*30*)

7 November 2013; accepted 15 January 2014
Published online 23 January 2014;
10.1126/science.1248215

Evolutionarily Dynamic Alternative Splicing of *GPR56* Regulates Regional Cerebral Cortical Patterning

Byoung-Il Bae,[1]* Ian Tietjen,[1]*† Kutay D. Atabay,[1] Gilad D. Evrony,[1] Matthew B. Johnson,[1] Ebenezer Asare,[1] Peter P. Wang,[1] Ayako Y. Murayama,[2] Kiho Im,[3] Steven N. Lisgo,[4] Lynne Overman,[4] Nenad Šestan,[5] Bernard S. Chang,[6] A. James Barkovich,[7] P. Ellen Grant,[3] Meral Topçu,[8] Jeffrey Politsky,[9]‡ Hideyuki Okano,[2] Xianhua Piao,[10] Christopher A. Walsh[1]§

The human neocortex has numerous specialized functional areas whose formation is poorly understood. Here, we describe a 15–base pair deletion mutation in a regulatory element of *GPR56* that selectively disrupts human cortex surrounding the Sylvian fissure bilaterally including "Broca's area," the primary language area, by disrupting regional *GPR56* expression and blocking RFX transcription factor binding. *GPR56* encodes a heterotrimeric guanine nucleotide–binding protein (G protein)–coupled receptor required for normal cortical development and is expressed in cortical progenitor cells. GPR56 expression levels regulate progenitor proliferation. *GPR56* splice forms are highly variable between mice and humans, and the regulatory element of gyrencephalic mammals directs restricted lateral cortical expression. Our data reveal a mechanism by which control of *GPR56* expression pattern by multiple alternative promoters can influence stem cell proliferation, gyral patterning, and, potentially, neocortex evolution.

Although most mammals have elaborate and species-specific patterns of folds ("gyri") in the neocortex, the genetic and evolutionary mechanisms of cortical gyrification are poorly understood (*1*–*3*). Abnormal gyrification, such as polymicrogyria (too many small gyri), invariably signals abnormal cortical development, so regional disorders of gyrification are of particular interest, because they highlight mechanisms specific to cortical regions. The human cortex contains dozens of cortical regions specialized for distinct functions—such as language, hearing, and sensation—yet it is unsolved how these cortical regions form and how human cortical regions evolved from those of prehuman ancestors.

Examination of >1000 individuals with gyral abnormalities identified five individuals from three

[1]Division of Genetics and Genomics, Manton Center for Orphan Disease, and Howard Hughes Medical Institute, Boston Children's Hospital, Broad Institute of MIT and Harvard, and Departments of Pediatrics and Neurology, Harvard Medical School, Boston, MA 02115, USA. [2]Department of Physiology, Keio University School of Medicine, Tokyo 160-8582, Japan. [3]Division of Newborn Medicine, Center for Fetal Neonatal Neuroimaging and Developmental Science, Department of Radiology, Boston Children's Hospital, Harvard Medical School, Boston, MA 02115, USA. [4]The MRC-Wellcome Trust Human Developmental Biology Resource (HDBR), Newcastle, Institute of Genetic Medicine, International Centre for Life, Central Parkway, Newcastle upon Tyne NE1 3BZ, UK. [5]Department of Neurobiology and Kavli Institute of Neuroscience, Yale University School of Medicine, New Haven, CT 06520, USA. [6]Beth Israel Deaconess Medical Center, Comprehensive Epilepsy Center, Boston, MA 02215, USA. [7]Departments of Radiology, Pediatrics, Neurology, and Neurological Surgery, University of California San Francisco, San Francisco, CA 94143, USA. [8]Department of Pediatrics, Hacettepe University Faculty of Medicine, Ankara, Turkey. [9]Department of Neurology, Medical College of Georgia, Augusta, GA 30912, USA. [10]Division of Newborn Medicine, Boston Children's Hospital and Harvard Medical School, Boston, MA 02115, USA.

*The authors contributed equally to this work.
†Present address: Department of Anesthesiology, Pharmacology and Therapeutics, University of British Columbia, Vancouver, British Columbia V6T 1Z4, Canada.
‡Present address: Northeast Regional Epilepsy Group, Atlantic Neuroscience Institute Epilepsy Center, Summit, NJ 07901, USA.
§Corresponding author. E-mail: christopher.walsh@childrens.harvard.edu

families (one Turkish and two Irish-American) with strikingly restricted polymicrogyria limited to the cortex surrounding the Sylvian fissure (Fig. 1, A and B; fig. S1; and movies S1 and S2), which suggests a rare, but genetically distinctive, condition. Affected individuals suffered intellectual and language difficulty, as well as refractory seizures (onset 7 months to 10 years), but had no motor disability (table S1). Magnetic resonance imaging (MRI) and quantitative gyral analysis showed abnormal inferior and middle gyri in prefrontal and motor cortex, with mildly affected temporal lobes. Broca's area—the "motor center for speech" (*4*)—in the left hemisphere and the corresponding areas of the right hemisphere were most severely affected. Affected neocortical surface showed abnormally numerous, small gyral-like folds that fused in coarse, irregular patterns, with abnormal and highly irregular white matter protrusions, consistent with polymicrogyria (*5*, *6*), along with widening of the Sylvian fissure (Fig. 1A and fig. S1B).

Genome-wide analysis identified a single linked locus on chromosome 16q12.2-21 (Fig. 1C) containing the *GPR56* gene, which, when mutated in its coding region, leads to polymicrogyria of the entire neocortex, as well as cerebellar and white matter abnormalities (*7*–*9*). As we found no mutations in the exons of *GPR56*, we sequenced 38 conserved non-exonic elements (table S2), in one of which we identified a small deletion in all five individuals. The mutated element normally contains two copies of a 15–base pair (bp) tandem repeat, but all affected individuals have a homozygous deletion of one 15-bp repeat (Fig. 1, E and F). The deletion is heterozygous in parents of the affected individuals, who manifest no obvious clinical signs, and is absent from thousands of control chromosomes in the Single-Nucleotide Polymorphism Database and 1000 Genomes database. The two Irish-American families carry the mutation on the same chromosomal haplotype, which reflects a common founder. It is noteworthy that the Turkish family carries the same deletion on a distinct haplotype, which indicates that the mutation arose independently (Fig. 1D). The element is located <150 bp upstream of the transcriptional start site of noncoding exon 1m (e1m) of *GPR56*, which suggests that it may regulate e1m expression as a cis-regulatory element. *GPR56* has at least 17 alternative transcription start sites, each beginning from a different noncoding first exon; all of the start sites are predicted to drive transcription of mRNAs whose coding sequence starts from exon 3 (Fig. 2A and fig. S2A) and all of which encode the same GPR56 protein (*10*, *11*). The diverse noncoding first exons have distinct expression profiles, with e1m being the most robustly transcribed first exon in fetal human brain but with several other alternative transcripts also expressed in fetal and adult brain (Fig. 2A and fig. S2, B to D).

To confirm that the 15-bp deletion disrupts perisylvian *GPR56* expression, we generated transgenic mice with the 23-kb human *GPR56* upstream region driving green fluorescent protein (GFP) expression. The 23-kb region encompasses 16 of the 17 transcription start sites containing e1m and ends before the translation start codon (Fig. 2A). This construct drives GFP expression in the entire central nervous system, including neocortex, and recapitulates the location and relative amount of expression of endogenous mouse GPR56 protein (Fig. 2B and fig. S3). In contrast, the 23-kb construct containing the 15-bp deletion drives expression in medial, but not lateral, cortex or lateral ganglionic eminence (Fig. 2B). These data suggest that the cis-regulatory element upstream of e1m drives *GPR56* expression in the perisylvian and lateral cortex, whereas disruption of the element, with consequent impairment of e1m expression, causes the perisylvian malformation.

To elucidate how the 15-bp deletion in the cis-regulatory element disrupts e1m expression,

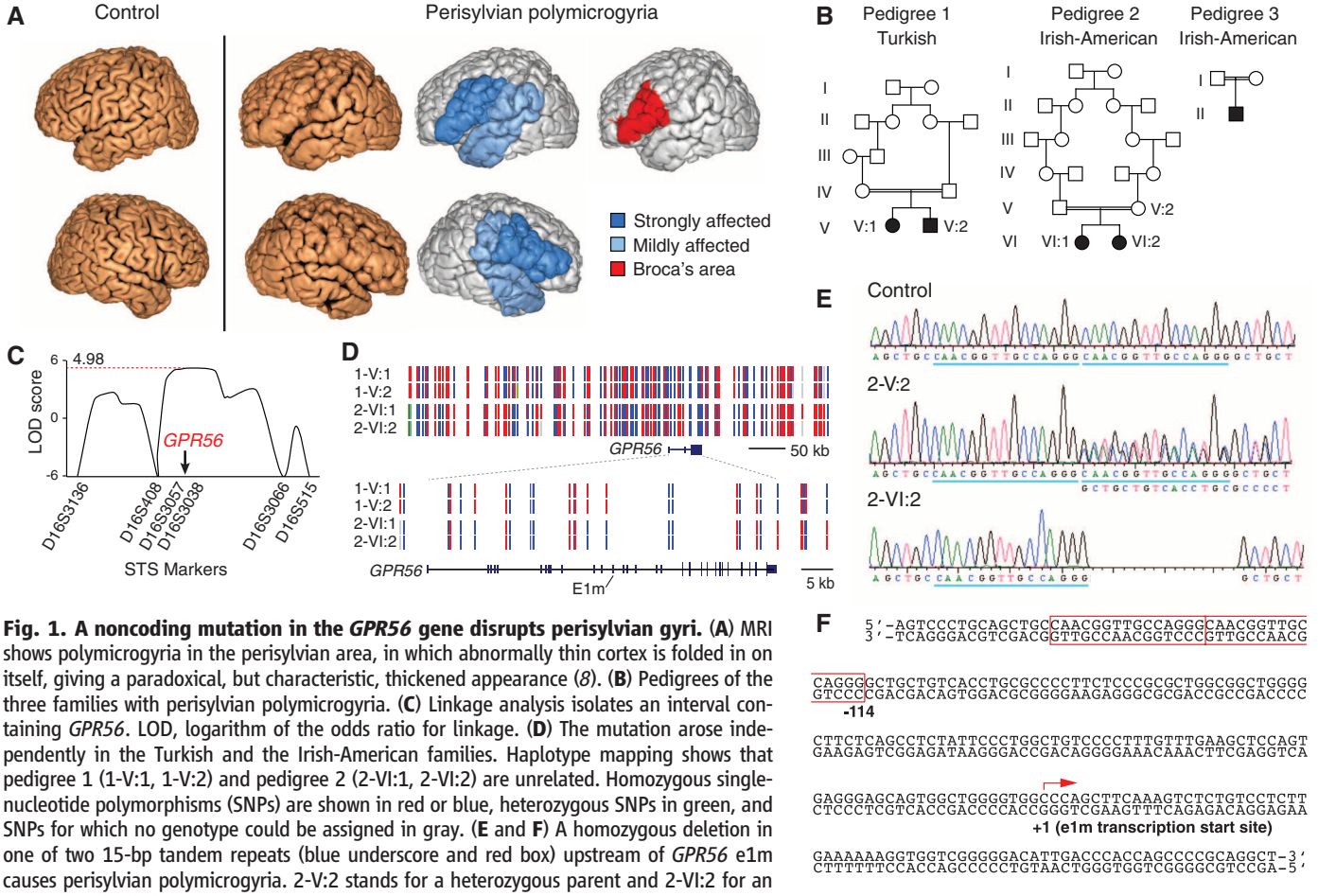

Fig. 1. A noncoding mutation in the *GPR56* gene disrupts perisylvian gyri. (**A**) MRI shows polymicrogyria in the perisylvian area, in which abnormally thin cortex is folded in on itself, giving a paradoxical, but characteristic, thickened appearance (*8*). (**B**) Pedigrees of the three families with perisylvian polymicrogyria. (**C**) Linkage analysis isolates an interval containing *GPR56*. LOD, logarithm of the odds ratio for linkage. (**D**) The mutation arose independently in the Turkish and the Irish-American families. Haplotype mapping shows that pedigree 1 (1-V:1, 1-V:2) and pedigree 2 (2-VI:1, 2-VI:2) are unrelated. Homozygous single-nucleotide polymorphisms (SNPs) are shown in red or blue, heterozygous SNPs in green, and SNPs for which no genotype could be assigned in gray. (**E** and **F**) A homozygous deletion in one of two 15-bp tandem repeats (blue underscore and red box) upstream of *GPR56* e1m causes perisylvian polymicrogyria. 2-V:2 stands for a heterozygous parent and 2-VI:2 for an affected individual from pedigree 2.

we performed yeast one-hybrid (Y1H) screening of a mouse forebrain cDNA library with the human cis-regulatory element as bait and obtained multiple yeast colonies encoding members of the *regulatory factor X (Rfx)* transcription factor family (Fig. 2C) (*12*). RFX1 and RFX3 bind the normal element in vitro, with binding decreased 60 to 70% by the 15-bp deletion (Fig. 2D). Chromatin immunoprecipitation sequencing confirmed RFX3 binding to the element (fig. S4) (*13*). RFX1 and GPR56 colocalize in germinal zones of fetal human brain (Fig. 2E). Dominant-negative RFX abrogates normal, but not mutant, e1m promoter activity on embryonic day 13.5 (E13.5) in mouse cortical cultures (Fig. 2F). Furthermore, genetic ablation of *Rfx4* decreases *Gpr56* expression in developing mouse brain (*14*). *RFX* and *GPR56* expression patterns are correlated (fig. S5, A and B) (*15*), with *RFX3* and *RFX7* most prominent in human ventrolateral prefrontal cortex, the region affected in perisylvian polymicrogyria (Fig. 2G), which suggests that multiple RFX proteins regulate the element.

GPR56 encodes an adhesion heterotrimeric guanine nucleotide–binding protein (G protein)–coupled receptor that is highly expressed in cortical progenitors (*7*, *16*) and binds extracellular matrix proteins (*17*). Loss of *GPR56* disrupts radial glia and causes breaches in the pial basement membrane, through which some neurons overmigrate (*9*, *16*). However, even where the pia is intact, we found that neocortical thickness and organization are irregular, with occasional thin regions in *Gpr56* knockout mice (Fig. 3A). Postmortem analysis of a human with biallelic *GPR56* coding mutations showed a very thin cortex, which suggested potential roles of *GPR56* in neurogenesis as well (*9*). GPR56 protein is most highly expressed in progenitors in the ventricular and subventricular zones during neurogenesis in mice (*16*, *18*). GPR56 expression in developing human and marmoset neocortex is highest in the ventricular zone, as well as in the outer subventricular zone, which is expanded in mammals with larger brains (*2*) (Fig. 3B and fig. S5, C and D).

Impairment and overexpression of *GPR56* show that its expression regulates proliferation. *Gpr56* knockout mice show fewer phosphohistone H3 (PH3)–positive mitotic progenitor cells and TBR2-positive intermediate progenitors than wild-type mice in the neocortex at E14.5. Conversely, mice carrying a transgene that directs overexpression of human *GPR56* show increased

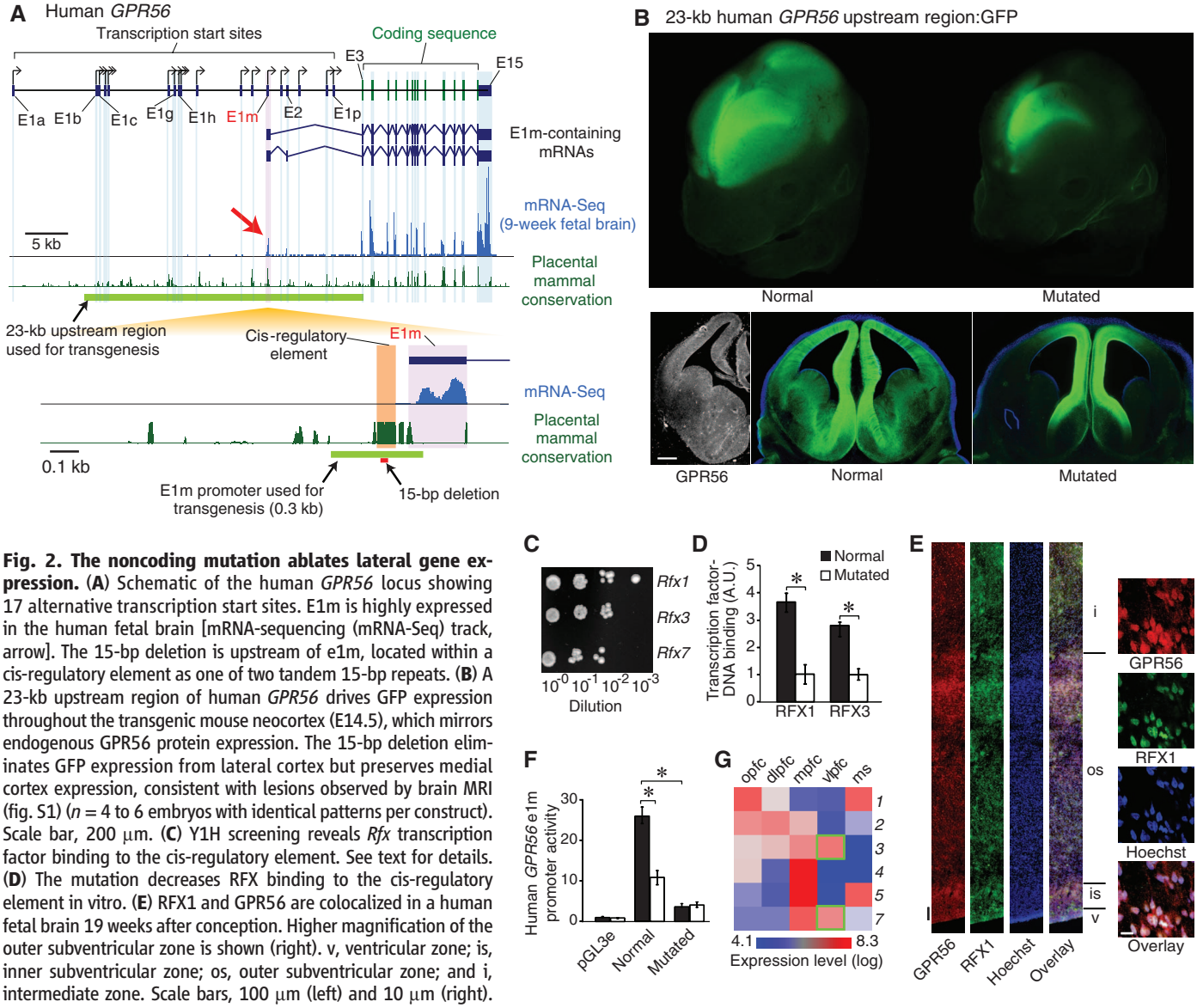

Fig. 2. The noncoding mutation ablates lateral gene expression. (**A**) Schematic of the human *GPR56* locus showing 17 alternative transcription start sites. E1m is highly expressed in the human fetal brain [mRNA-sequencing (mRNA-Seq) track, arrow]. The 15-bp deletion is upstream of e1m, located within a cis-regulatory element as one of two tandem 15-bp repeats. (**B**) A 23-kb upstream region of human *GPR56* drives GFP expression throughout the transgenic mouse neocortex (E14.5), which mirrors endogenous GPR56 protein expression. The 15-bp deletion eliminates GFP expression from lateral cortex but preserves medial cortex expression, consistent with lesions observed by brain MRI (fig. S1) ($n = 4$ to 6 embryos with identical patterns per construct). Scale bar, 200 μm. (**C**) Y1H screening reveals *Rfx* transcription factor binding to the cis-regulatory element. See text for details. (**D**) The mutation decreases RFX binding to the cis-regulatory element in vitro. (**E**) RFX1 and GPR56 are colocalized in a human fetal brain 19 weeks after conception. Higher magnification of the outer subventricular zone is shown (right). v, ventricular zone; is, inner subventricular zone; os, outer subventricular zone; and i, intermediate zone. Scale bars, 100 μm (left) and 10 μm (right). (**F**) Dominant-negative RFX (white bars) abrogates normal e1m promoter activity. Black bars, GFP control. (**G**) Each *RFX* gene has distinct expression patterns in the fetal human brain. Each number means the corresponding *RFX* isoform. *RFX3* and *RFX7* are enriched in regions affected by perisylvian polymicrogyria (green boxes). pfc, prefrontal cortex; opfc, orbital pfc; dlpfc, dorsolateral pfc, mpfc, medial pfc; vlpfc, ventrolateral pfc; ms, motor-sensory cortex. *$P < 0.001$, *t* test.

mitotic progenitor cells and intermediate progenitor cells (Fig. 3, C and D). In utero electroporation (at E13.5 with analysis 48 hours later at E15.5) of a plasmid encoding *GPR56* (as well as GFP, to mark the cells) caused cells to persist in proliferative zones compared with cells expressing GFP alone (Fig. 3E). Changes in the number of intermediate progenitors in transgenic and knockout mice may be secondary to changes in the radial progenitor cells that generate them or might reflect a direct role of GPR56 in intermediate progenitors but is consistent with a report that loss of *TBR2* (*EOMES*) also causes polymicrogyria in humans (*19*).

The cis-regulatory element upstream of *GPR56* e1m is found in genomes of all placental mammals, but not monotremes, marsupials, or nonmammals, which suggests that it emerged after placental and nonplacental mammals diverged 85 to 100 million years ago (fig. S7B). The cis-regulatory element sequence is only found at the e1m locus in *GPR56* but not elsewhere in the genome. E1m itself shows homology at its 3′ end to a long interspersed nuclear element (LINE)–4/RTE, a family of retrotransposons active in early mammals after divergence from marsupials (*20*). Another noncoding *GPR56* exon (exon 2), present only in primates, derives from a primate-specific *Alu* insertion (fig. S7B). In contrast to the >17 alternative first exons in humans, we found only five noncoding first exons in the mouse *Gpr56* gene (Fig. 4A and fig. S7A) (*10*, *11*). Thus, *GPR56* acquired many noncoding upstream exons and generated alternative splice forms with distinct expression patterns (fig. S2, B and D), in the lineage leading to humans. Transposable element insertion played a role in generating this diversity.

To test directly whether evolutionary changes in *GPR56*'s alternative splice forms have functional effects, we generated transgenic mice in which the β-galactosidase (β-gal) gene is driven by a minimal 300-bp e1m promoter from human, mouse, marmoset, dolphin, and cat (Fig. 2A and fig. S6A). The mouse e1m promoter drives β-gal expression broadly in the nervous system in diverse cell types, which suggests that this simple 300-bp e1m promoter is sufficient to recapitulate major features of the endogenous mouse GPR56 expression (*16*–*18*) (Fig. 4B and fig. S6B). In contrast, the corresponding human e1m promoter has a variety of deletions and single-nucleotide variants, relative to the mouse sequence (fig. S6A), and drives much more limited expression in rostral-lateral cortex (Fig. 4B and fig. S6B). Weak lateral cortical expression is visible in embryos carrying the mouse e1m promoter:β-gal transgene,

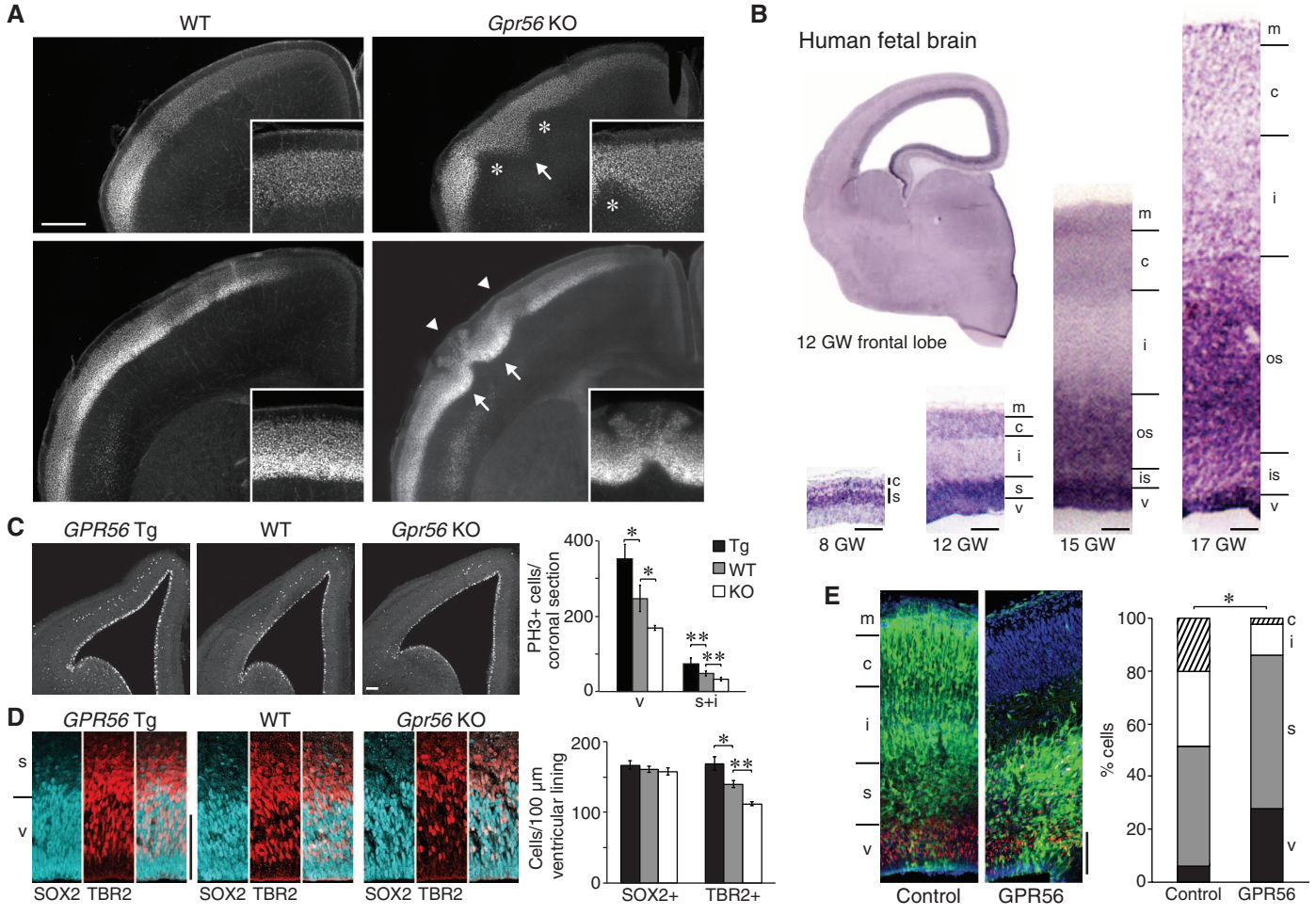

Fig. 3. GPR56 regulates neuroprogenitor proliferation. (**A**) In *Gpr56* knockout mice, neurons overmigrate through breached pial basement membrane (arrowheads) or undermigrate (arrows) forming irregular cortical layers, as shown by immunostaining of Cux1, an upper layer (II to IV) marker (p9). Thin cortex is occasionally observed (asterisks). (**B**) *GPR56* is highly expressed in human ventricular zone and outer subventricular zone at 12 to 17 weeks of gestation (GW), which suggests roles in neuroprogenitors. v, ventricular zone; s, subventricular zone; is, inner subventricular zone; os, outer subventricular zone; i, intermediate zone; c, cortical plate; and m, marginal zone. (**C** to **D**) Human *GPR56* transgenic (Tg) mice have significantly more mitotic (PH3+) neuroprogenitor cells and intermediate progenitor (TBR2+) cells than wild-type (WT). In contrast, *Gpr56* knockout (KO) mice have significantly fewer mitotic cells and intermediate progenitors than WT (E13.5 to E14.5). (n = 7 mice per genotype; *P < 0.005; **P < 0.001; paired t test). (**E**) The cells that are in utero electroporated (from E13.5 to E15.5) with human *GPR56*-IRES-GFP [either side of the internal ribosome entry site (IRES), GFP expressing] persist in the germinal zones longer that the GFP control cells. Red, TBR2; blue, Hoechst. (n = 11 mouse embryos per construct; *P < 0.0001; chi-squared test). Scale bars, 500 μm (A) and 100 μm (B) to (E).

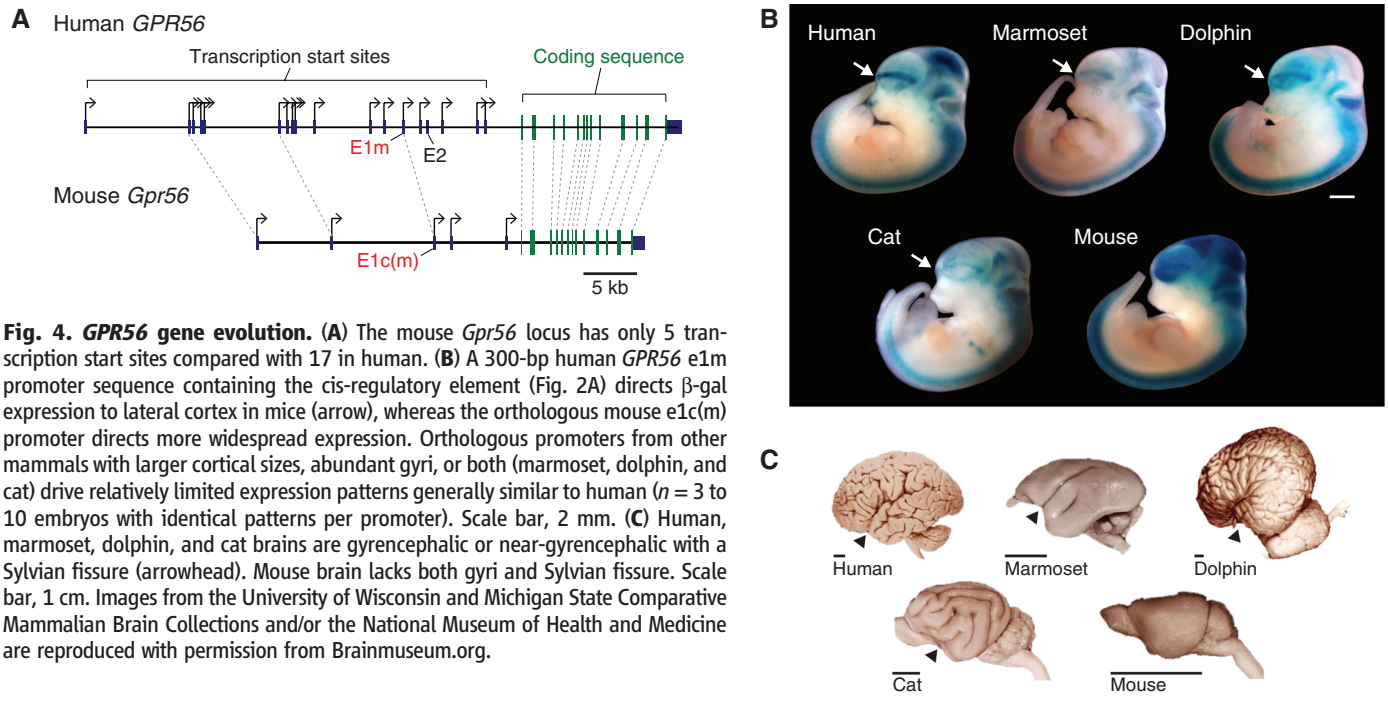

Fig. 4. *GPR56* gene evolution. (**A**) The mouse *Gpr56* locus has only 5 transcription start sites compared with 17 in human. (**B**) A 300-bp human *GPR56* e1m promoter sequence containing the cis-regulatory element (Fig. 2A) directs β-gal expression to lateral cortex in mice (arrow), whereas the orthologous mouse e1c(m) promoter directs more widespread expression. Orthologous promoters from other mammals with larger cortical sizes, abundant gyri, or both (marmoset, dolphin, and cat) drive relatively limited expression patterns generally similar to human ($n = 3$ to 10 embryos with identical patterns per promoter). Scale bar, 2 mm. (**C**) Human, marmoset, dolphin, and cat brains are gyrencephalic or near-gyrencephalic with a Sylvian fissure (arrowhead). Mouse brain lacks both gyri and Sylvian fissure. Scale bar, 1 cm. Images from the University of Wisconsin and Michigan State Comparative Mammalian Brain Collections and/or the National Museum of Health and Medicine are reproduced with permission from Brainmuseum.org.

which suggests that, in humans, additional elements besides the 300-bp e1m promoter region are required to drive the full complement of *GPR56* expression. E1m promoters from marmoset, dolphin, and cat drive expression patterns generally similar to human. The shared expression patterns in the four mammals that have a Sylvian fissure (Fig. 4C) suggest that elaboration of *GPR56* noncoding regulation is consistent with the larger number of noncoding first exons in gyrencephalic mammals and humans. Elaboration of additional alternative splice forms provides a mechanism for potentially independent evolution of these multiple forms.

Our studies show that levels of *GPR56* control proliferation of progenitors in the neocortex. Loss of *GPR56* expression impairs neurogenesis, and overexpression enhances proliferation and progenitor number. Selective *GPR56* loss causes strikingly regional defects of cortical development. *GPR56* likely influences progenitor proliferation by stabilizing the basal process of radial neuroepithelial progenitors, because (i) GPR56 protein localizes to the basal processes of radial neuroepithelial cells (*16*); (ii) GPR56 binds extracellular matrix proteins in the pial basement membrane, such as collagen type III (*17*) and tetraspanins, which bind integrins as well (*21*); (iii) GPR56 is required for normal attachment of basal processes to the pial basement membrane in mice (*16*); and (iv) basal processes regulate progenitor proliferation via integrin signaling (*22*, *23*), and *GPR56* interacts genetically with $\alpha_3\beta_1$ integrin (*24*). The elaboration of the *GPR56* locus in gyrencephalic mammals, and especially humans, to produce many alternative splice forms with diverse expression patterns presents *GPR56* as a key target that could influence the dramatic changes in shape and folding that characterize the forebrain of many mammals. Elaboration and specialization of alternative transcripts with distinct transcription start sites is an evolutionary mechanism that has been difficult to study because of the lack of comprehensive catalogs of RNA splice forms, but continued RNA sequencing studies may soon provide the opportunity to assess its importance systematically.

References and Notes

1. P. Rakic, *Nat. Rev. Neurosci.* **10**, 724–735 (2009).
2. J. H. Lui, D. V. Hansen, A. R. Kriegstein, *Cell* **146**, 18–36 (2011).
3. K. Zilles, N. Palomero-Gallagher, K. Amunts, *Trends Neurosci.* **36**, 275–284 (2013).
4. K. Amunts *et al.*, *PLOS Biol.* **8**, e1000489 (2010).
5. J. A. Golden, B. N. Harding, *Nat. Rev. Neurol* **6**, 471–472 (2010).
6. A. J. Barkovich, *Neuroradiology* **52**, 479–487 (2010).
7. X. Piao *et al.*, *Science* **303**, 2033–2036 (2004).
8. X. Piao *et al.*, *Ann. Neurol.* **58**, 680–687 (2005).
9. N. Bahi-Buisson *et al.*, *Brain* **133**, 3194–3209 (2010).
10. D. Thierry-Mieg, J. Thierry-Mieg, *Genome Biol.* **7** (suppl. 1), S12–S14 (2006).
11. Y. Suzuki, R. Yamashita, K. Nakai, S. Sugano, *Nucleic Acids Res.* **30**, 328–331 (2002).
12. S. J. Ansley *et al.*, *Nature* **425**, 628–633 (2003).
13. A. Jolma *et al.*, *Genome Res.* **20**, 861–873 (2010).
14. D. Zhang *et al.*, *J. Neurochem.* **98**, 860–875 (2006).
15. H. J. Kang *et al.*, *Nature* **478**, 483–489 (2011).
16. S. Li *et al.*, *J. Neurosci.* **28**, 5817–5826 (2008).
17. R. Luo *et al.*, *Proc. Natl. Acad. Sci. U.S.A.* **108**, 12925–12930 (2011).
18. S. J. Jeong, R. Luo, S. Li, N. Strokes, X. Piao, *J. Comp. Neurol.* **520**, 2930–2940 (2012).
19. L. Baala *et al.*, *Nat. Genet.* **39**, 454–456 (2007).
20. T. S. Mikkelsen *et al.*, *Nature* **447**, 167–177 (2007).
21. L. Xu, R. O. Hynes, *Cell Cycle* **6**, 160–165 (2007).
22. R. Radakovits, C. S. Barros, R. Belvindrah, B. Patton, U. Müller, *J. Neurosci.* **29**, 7694–7705 (2009).
23. S. A. Fietz *et al.*, *Nat. Neurosci.* **13**, 690–699 (2010).
24. S. J. Jeong *et al.*, *PLOS ONE* **8**, e68781 (2013).

Acknowledgments: Research performed on samples of human origin was conducted according to protocols approved by participating institutions, including Boston Children's Hospital and Beth Israel Deaconess Medical Center. The human embryonic and fetal material was provided by the Joint Medical Research Council (grant no. G0700089)–Wellcome Trust (grant no. GR082557) Human Developmental Biology Resource (www.hdbr.org) and the National Institute of Child Health and Human Development, NIH, Brain and Tissue Bank at the University of Maryland (contract no. HHSN275200900011C, reference no. NO1-HD-9-0011). *Gpr56* knockout mice are from Genentech. This work was supported by the Strategic Research Program for Brain Sciences and from the Ministry of Education, Culture, Sports, Science and Technology (MEXT) Japan (H.O.); Funding Program for World-Leading Innovative R&D on Science and Technology (FIRST Program) (H.O.); U01MH081896 from National Institute of Mental Health, NIH (N.S.); 2R01NS035129 from National Institute of Neurological Disorders and Stroke, NIH (C.A.W.); and The Paul G. Allen Family Foundation (C.A.W.). Additional funding support listed in supplementary materials. C.A.W. is an investigator of the Howard Hughes Medical Institute. *Gpr56* knockout mice are available from Genentech subject to a Material Transfer Agreement.

Supplementary Materials

www.sciencemag.org/content/343/6172/764/suppl/DC1
Materials and Methods
Supplementary Text
Figs. S1 to S7
Tables S1 and S2
Movies S1 to S2
References (*25*–*40*)

7 August 2013; accepted 17 December 2013
10.1126/science.1244392

Supplementary Materials for

Evolutionarily Dynamic Alternative Splicing of GPR56 Regulates Regional Cerebral Cortical Patterning

Byoung-Il Bae, Ian Tietjen, Kutay D. Atabay, Gilad D. Evrony, Matthew B. Johnson, Ebenezer Asare, Peter P. Wang, Ayako Y. Murayama, Kiho Im, Steven N. Lisgo, Lynne Overman, Nenad Šestan, Bernard S. Chang, A. James Barkovich, P. Ellen Grant, Meral Topçu, Jeffrey Politsky, Hideyuki Okano, Xianhua Piao, Christopher A. Walsh*

*Corresponding author. E-mail: christopher.walsh@childrens.harvard.edu

Published 14 February 2014, *Science* **343**, 764 (2014)
DOI: 10.1126/science.1244392

This PDF file includes

Other Supplementary Material for this manuscript includes the following:
(available at www.sciencemag.org/content/343/6172/764/suppl/DC1)

Movies S1 and S2

Materials and Methods

Human genetics

All affected individuals and magnetic resonance images (MRIs) were examined by neurologists, and BFPP or perisylvian polymicrogyria was diagnosed using criteria described here and previously (*25, 26*). An autosomal recessive genetic model was assumed with a susceptibility allele frequency of 0.001 and penetrance 0.99. SNP analysis was performed with Affymetrix genome-wide human SNP array 6.0. For Pedigree 2, a 10-cM average genome-wide screen was performed using ~400 fluorophore-labeled PCR primers spanning polymorphic microsatellite regions. The following microsatellite markers were analyzed: *D16S3044*, *D16S540*, *D16S3136*, *D16S3034*, *D16S415*, *D16S408*, *D16S3057*, *D16S3038*, *D16S3094*, *D16S3132*, *D16S514*, *D16S503*, *D16S3067*, *D16S3066*, *D16S3040*, *D16S505*, and *D16S3091*. LOD scores were determined using GeneHunter and Allegro statistical software (*27*). For each marker, four alleles at equal frequencies were assumed. Chromosomal regions of interest were subsequently analyzed with additional microsatellite PCR primers. Each *GPR56* exon or conserved noncoding element plus >100 bp of flanking genomic sequence was sequenced, to identify the mutation. Control DNAs were obtained from healthy individuals of Arabic (n = 40), European (n = 200), and Turkish (n = 120) descent (Coriell Human Variation Panels), the dbSNP database, and the 1000 Genomes database.

Quantitative MRI analysis

The MRI images (individuals VI:1 and VI:2 of pedigree 2 and control age-matched control subjects) were processed to extract the surfaces of the gray/white matter and gray matter/cerebrospinal fluid boundaries, and to define Brodmann areas on the cortical surface using the FreeSurfer software (*28*). Quantitative comparison of sulcal patterns (*29*) in the left and right lobes revealed that perisylvian cortex including frontal and temporal lobes are abnormal in the individuals with perisylvian polymicrogyria. Medial lobes are normal.

mRNA-Seq

A 9 post-conceptual week fetal human brain was obtained at Human Developmental Biology Resource at Newcastle University. The brain was snap-frozen, sectioned with a vibratome at 200 μm, stored in RNAlater-ICE (Ambion) at -70 °C, which were then microdissected to isolate lateral cortical tissue. Mouse cortex was dissected fresh from E12.5 embryos. RNA was isolated using the mirVana kit (Ambion). mRNA was purified using the Oligotex mRNA Mini kit (Qiagen), and a barcoded sequencing library preserving strand-information was prepared with the SOLiD Whole Transcriptome Analysis Kit (Applied Biosystems). The libraries were sequenced to a depth of 140-175 million reads on the SOLiD Plus sequencing system. Reads were mapped using Bioscope software (Applied Biosystems) to the genome reference (hg18 and mm9) and splice-junctions obtained from the UCSC Genes annotation track (*30*).

BrainSpan data analysis

GPR56 e1m (chr16:57673206-57673582, GRCh37/hg19) RNA-seq expression measured in RPKM (reads per kilobase exon per million mapped reads) was obtained from the BrainSpan project data (Allen Brain Atlas) and summarized to Gencode v10 exons for all annotated neocortex tissues aged 8 post conception week to 1 year.

Mouse transgenesis

Transgenic mice were generated using bacterial artificial chromosome (BAC) recombineering (*31*) and piggyBac transposase system (*32*). A BAC clone containing human *GPR56* (RP11-78C18) was purchased from Children's Hospital Oakland Research Institute. The 15-bp deletion was introduced into the cis-regulatory element upstream of e1m using galK-based BAC recombineering. For reporter gene expression, EGFP and *lacZ* followed by SV40 late poly(A) signal and SV40 enhancer were inserted into pCyL50 piggyBac plasmid. Normal and mutated 23-kb *GPR56* promoters (chr16:56,218,517-56,241,700 (hg18)) were retrieved into the pCyL50-EGFP vector using 500-bp homology arms, so that the promoters can drive EGFP expression. *GPR56* e1m promoters from human (chr16: 56,230,630-56,230,943 (hg18)) and mouse (chr8:97,517,950-97,518,280 (mm9)) were PCR amplified from genomic DNA, and marmoset, cat, and dolphin promoters were synthesized (Genewiz), and inserted into the pCyL50-lacZ vector. For *GPR56* transgenic mice, we used pCAG-human *GPR56* cDNA-IRES-EGFP-rabbit globin poly(A) construct that was cloned into pCyL50 plasmid. All constructs were prepared with Pureyield endotoxin free midiprep kit (Promega), linearized by NotI or AloI digestion, and purified with Wizard DNA clean-up system (Promega). HyPBase mRNA was synthesized with mMessage mMachine mRNA T7 Transcription Kit (Ambion), and purified using NucAway spin columns (Ambion). 20 ng/μl hyPBase mRNA and 2 ng/μl linear plasmid were microinjected into fertilized FVB/N eggs following protocols approved by the Brigham and Women's Hospital. We obtained 4-10 independent embryos with highly similar staining patterns from each construct. Transgenic mice and non-transgenic control littermates were analyzed for each experiment.

Ferret electroporation

5-kb human *GPR56* e1m promoter (chr16:56,225,866-56,230,943 (hg18)) was cloned into pCyL50-EGFP vector and used for electroporations. Ferrets (*Mustela putorius furo*) were obtained from Marshall Bioresources. P0 ferret kits were anesthetized with 5% isoflurane and maintained at 3% utilizing a nose cone during the entire procedure. A small incision was made on the skin at the dorsomedial part of the head using a surgical blade and a hole was opened anterior to the bregma on the left side of the skull, on top of the lateral ventricle using an insulin needle. 3-5μl (1 μg/μl) of the construct was injected to the lateral ventricle using a pulled glass micropipette. 150V electric pulses were passed 5 times with 1s intervals using an electroporator. The incision was closed using VetBond (3M) tissue adhesive and kits were returned to the nest after reanimation. Brains were harvested on P7 after a transcardial perfusion and drop-fixed in 4% PFA overnight.

In utero electroporation of mouse embryos

pCAG-human *GPR56* cDNA-IRES-EGFP or pCAG-EGFP (1 μg/μl) were electroporated *in utero* into the ventricles of mouse embryos at e13.5 as previously described (*33*). At e15.5, successfully electroporated embryos were detected based on EGFP fluorescence and analyzed by immunohistochemistry after vibratome sectioning. EGFP-positive cells in each layer were manually counted and the distributions of the cells were compared using Chi-squared test.

Immunohistochemistry and *in situ* hybridization

Animals were perfused with 4% cold PFA in PBS and the brains were drop-fixed for 8 hours in 4% PFA at 4°C. For cryosections, brains were placed in 30% sucrose in PBS overnight for cryopreservation, and sectioned at 16μm thickness. Free-floating sections were embedded in 4% low-melting agarose and sectioned at 75μm. Antigen retrieval was performed on slide-mounted cryo-tissue by autoclaving the sections for 8 minutes in Retrievagen-A Solution (pH 6.0) (BD Biosciences). Sections were blocked in a solution containing 10% normal donkey serum (Jackson ImmunoResearch) and 0.1% Triton X-100. Sections were incubated in primary antibody solution containing the primary antibodies, 5% fetal donkey serum and 0.05% Triton X-100 overnight at 4°C. Free-floating sections were permeabilized and blocked in a solution containing 3% bovine serum albumin (Sigma), 0.02% Triton X-100 overnight at 4°C. Following primary and secondary antibody incubations were performed using the same permeabilization/blocking solution for free-floating sections, each overnight at 4°C. Primary antibodies included mouse anti-phosphorylated Vimentin (4A4) 1:500 (MBL), rabbit anti-Phosphohistone H3 (Ser10) 1:500 (Millipore), rabbit anti-CUX1 (CDP) 1:500 (Santa Cruz), goat anti-RFX1 (I-19) 1:100 (Santa Cruz), chicken anti-TBR2 1:500 (Millipore), goat anti-SOX2 1:250 (Santa Cruz), mouse anti-GPR56 1:250 (Millipore), rabbit anti-GPR56 1:250 (*16*), and rabbit anti-β-galactosidase 1:500 (MP Biomedicals). Sections were rinsed in PBS, then incubated for two hours at RT in secondary antibody buffer containing the secondary antibodies in 5% fetal donkey serum, 0.05% Triton X-100. Secondary antibodies included AlexaFluor (488nm and 563nm) donkey anti-mouse and donkey anti-rabbit (Invotrogen). Slices were then rinsed and coverslipped with Fluoromount-G (Southern Biotech) containing Hoechst 1:1000 (Roche). *In situ* hybridization was performed as previously described (*7, 34-36*). Images were obtained with Zeiss LSM700 confocal microscope and Leica MZ16 F fluorescence stereomicroscope. For statistical analysis of PH3-positive, SOX2-positive, and TBR2-positive cells, we selected only matching sections and fields from GPR56 transgenic, WT, and Gpr56 knockout mice. After counting all the PH3-positive cells in the chosen fields, paired t-test was performed.

Luciferase assay

Human *GPR56* e1m promoter (chr16:56,230,630-56,230,943 (hg18)) with or without the mutation was cloned into pGL3-Enhancer (pGL3e) vector (Promega), and the luciferase activity was measured after electroporation (Amaxa nucleofector system, Lonza) into e13 mouse primary cortical culture. Mouse *Rfx1* DNA binding domain (400-527 aa) was used as the dominant negative RFX (*37*).

Yeast one-hybrid assay

Using the conserved sequence from the cis-regulatory element upstream of human *GPR56* e1m (chr16:56,230,778-56,230,841 (hg18)) as a bait and *HIS3* as a selection marker, we screened E13 mouse forebrain cDNA library in Y187 strain at 25 mM of 3-amino-1,2,4-triazole (Clontech).

In vitro protein-DNA binding assay

Intact and mutant e1m promoters were PCR-amplified, biotinylated on one end, incubated with cellular extracts containing ProLabel-tagged Rfx, and captured on a streptavidin-coated 96-well plate. After washing, specific protein-DNA binding interactions were calculated based on the ProLabel-tag activity (Clontech).

Human brain exon array heatmaps

Normalized log expression levels of *RFX1-7* were obtained from Affymetrix exon 1.0 ST array analyses of four late mid-fetal human brains (18, 19, 21, and 23 weeks of gestation) as described previously (*38*). Heatmaps were generated using Java Tree-view. To determine which *RFX* genes are most highly correlated with human *GPR56*, we used previously generated dataset for pairwise Pearson comparisons, available from www.humanbraintranscriptome.org. It covers 16 brain cortical regions over 15 periods, ranging in stage from embryonic development to late adulthood. The evaluation of gene expression in each region and each period is detailed elsewhere (*15*). Here, we averaged gene expression values of 16 brain regions in each of 15 periods represented in the data set, and then performed pairwise Pearson correlation analysis for *GPR56* and the members of the *RFX* family. The correlation analysis was shown by heatmap and the correlation coefficients were indicated in each cell.

ChIP-Seq analysis

Raw reads of RFX3 ChIP-Seq (*13*) were obtained from the NCBI Short Read Archive, specifically the SRX017474 (RFX3 sc-10662 antibody ChIP-Seq in K562 cells) and SRX017477 (IgG control ChIP-Seq in K562 cells) datasets. Reads were mapped using bowtie (*39*) using default parameters to hg18. Mapped reads were visualized in the UCSC genome browser.

Analysis of *GPR56* evolution

Ensembl, NCBI, and UCSC genome bioinformatics data were checked for presence of *GPR56* e1m cis-element, e2, and coding sequence orthologues in other species. The evolutionary tree was generated using the interactive tree of life, iTOL (*40*).

Supplementary Text

Further Acknowledgements

We thank Brenda Barry, Jennifer Partlow, Kathryn Allen, Kira Apse, Adria Bodell, Christina Austin, the DFCC Microarray Core Facility, Victoria Petkova, Danielle Gleason, Rui Zhou, In Situ Hybridization Core Facility of the University of North Carolina at Chapel Hill, Brigham and Women's Hospital Transgenic Core Facility, Jordan P. Amadio, Xuyu Cai, Divya Jayaraman, and Diana Flanagan for technical assistance; Dilenny Gonzalez for in utero electroporation; William B. Dobyns, Jane Roskams, and the Roskams lab for discussions and support; the Center for Inherited Disease Research (CIDR) for genotyping; Rong Luo for technical advice on immunohistochemistry; Qiufu Ma for Rfx *in situ* hybridization probe constructs; Hiroaki Kanki, Fumiko Ozawa and Misako Okuno for technical support to *in situ* hybridization of marmoset brain; Wellcome Trust Sanger Institute for pCyl50 and pCMV-hyPBase plasmids; David Beier, Bryan Bjork, and Margaret Thompson for discussion on piggyBac-based mouse transgenesis; Tarjei Mikkelsen and David Haussler for discussion on evolution of *GPR56*. BrainSpan data are from the website of Allen Institute for Brain Science, BrainSpan Atlas of the Developing Human Brain [Internet], which is available from: http://brainspan.org/ ©2012. The brain images from different species were reproduced with permission from http://www.brains.rad.msu.edu, and http://brainmuseum.org, supported by the US National Science Foundation. This work was supported by Boston Children's Hospital Developmental Neurology Training Grant T32NS007473 (B.-I.B.), Harvard Stem Cell Institute Training Grant T32HL087735-01A1 (B.-I.B.), Harvard Medical School Goldenson Fellowship (B.-I.B.), Kirschstein-NRSA Individual Postdoctoral Fellowship from NICHD F32HD048035 (I.T.), NIH MSTP grant T32GM007753 (G.D.E.) and the Louis Lange III Scholarship in Translational Research (G.D.E.). CIDR is funded through a federal contract from the National Institutes of Health to the Johns Hopkins University (contract number N01-HG-65403).

Author Contributions

M.T. identified the Turkish family, and J.P., the Irish Travellers families. B.S.C., A.J.B., K.I., P.E.G., and C.A.W. examined the MRI. K.I. and P.E.G. created the 3D renderings of outer cortical surface and gray-white junction, and performed sulcal pattern analysis. With X.P. and C.A.W., I.T. analyzed human genetics data and identified the noncoding mutation. B.-I.B., I.T., and G.D.E. analyzed mRNA-Seq, ChIP-Seq, and BrainSpan data. B.-I.B., I.T., G.D.E., and C.A.W. examined *GPR56* evolution. B.-I.B. performed luciferase assays, and Y1H assays, and generated all constructs and transgenic mice. B.-I.B., E.A., and K.D.A. analyzed the transgenic and *Gpr56* knockout mice by immunohistochemistry. S.N.L. and L.O. did human brain *in situ* hybridization. A.M. and H.O. performed marmoset *in situ* hybridization. K.D.A., M.B.J., and P.P.W. injected ferrets and performed immunohistochemistry. M.B.J. and N.Š. analyzed *RFX* expression patterns in the human fetal brains. B.-I. B, I.T., and C.A.W. wrote the manuscript, and all the co-authors critically reviewed multiple times. The authors declare no competing financial interests.

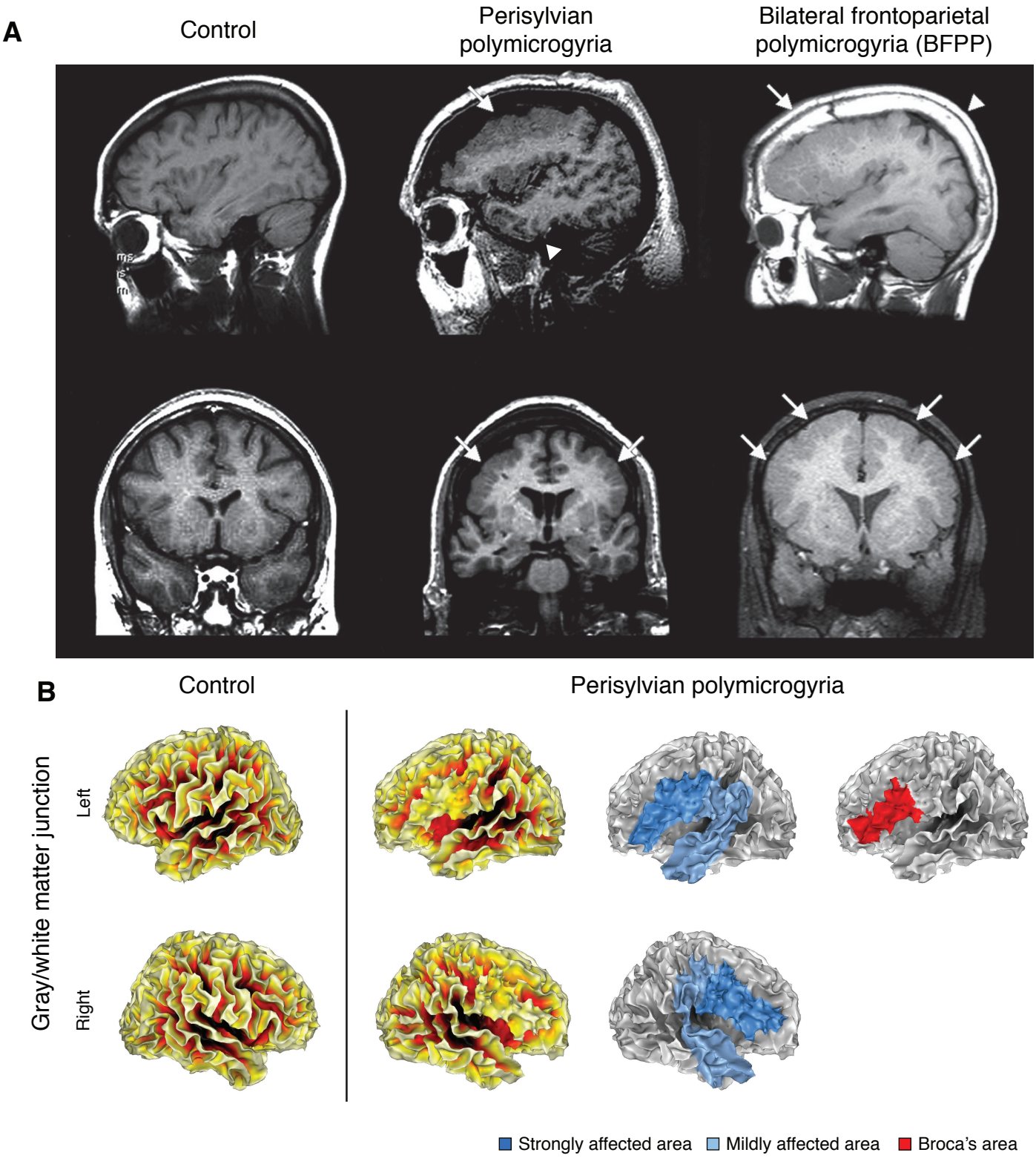

Fig. S1. Anatomical phenotype of perisylvian polymicrogyria. **(A)** Magnetic resonance imaging (MRI) of individuals with perisylvian polymicrogyria, bilateral frontoparietal polymicrogyria (BFPP), and a control individual. Arrows demarcate severely affected area, and arrowheads mildly affected area. This particular BFPP is caused by *GPR56*-null mutation, and perisylvian polymicrogyria by the 15-bp deletion in the cis-regulatory element upstream of e1m. The medial parts of the perisylvian polymicrogyria brain are intact. **(B)** 3-dimentional reconstruction of gray matter-white matter junction based of MRI on perisylvian polymicrogyria brain reveal an abnormal, "scalloped" appearance in the perisylvian gyri.

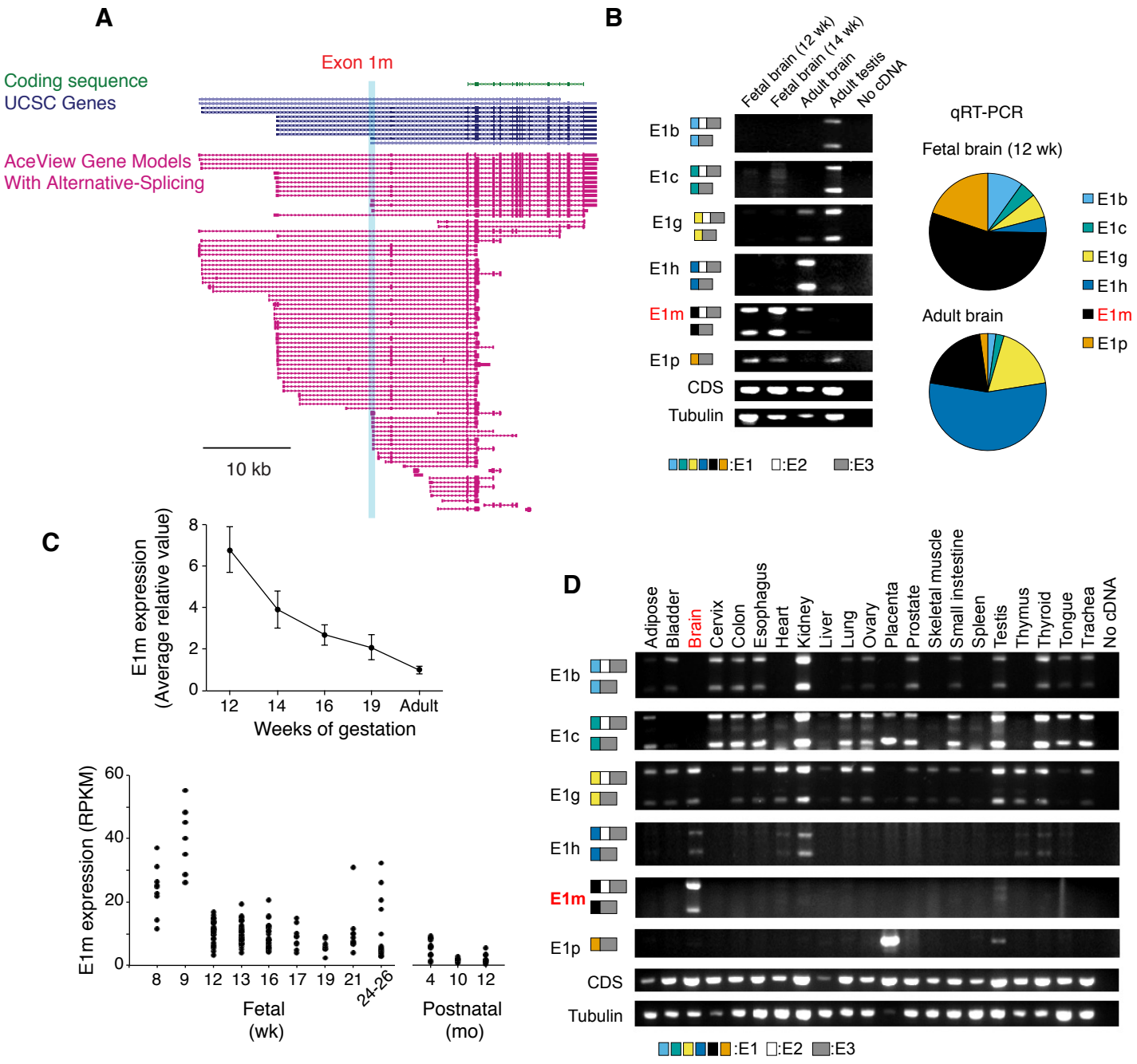

Fig. S2. Expression patterns of different first exons of human *GPR56*. **(A)** Human has about 80 alternative splice variants of *GPR56*, according to the AceView database. **(B)** RT-PCR from human fetal and adult brains shows that e1m is highly expressed in fetal brain, with other splice forms expressed in adult brain. E1p, which is absent in mice, is also expressed in the fetal human brain. Some *GPR56* splice forms generate two PCR products that reflect the differential presence of e2. **(C)** E1m is expressed in the brain throughout fetal development, as shown by qRT-PCR (mean+/-SEM) (top) and the BrainSpan project data (Allen Brain Atlas) (bottom). RPKM, reads per kb exon per million mapped reads. **(D)** Each exon 1 has a unique expression pattern in different types of adult human tissues.

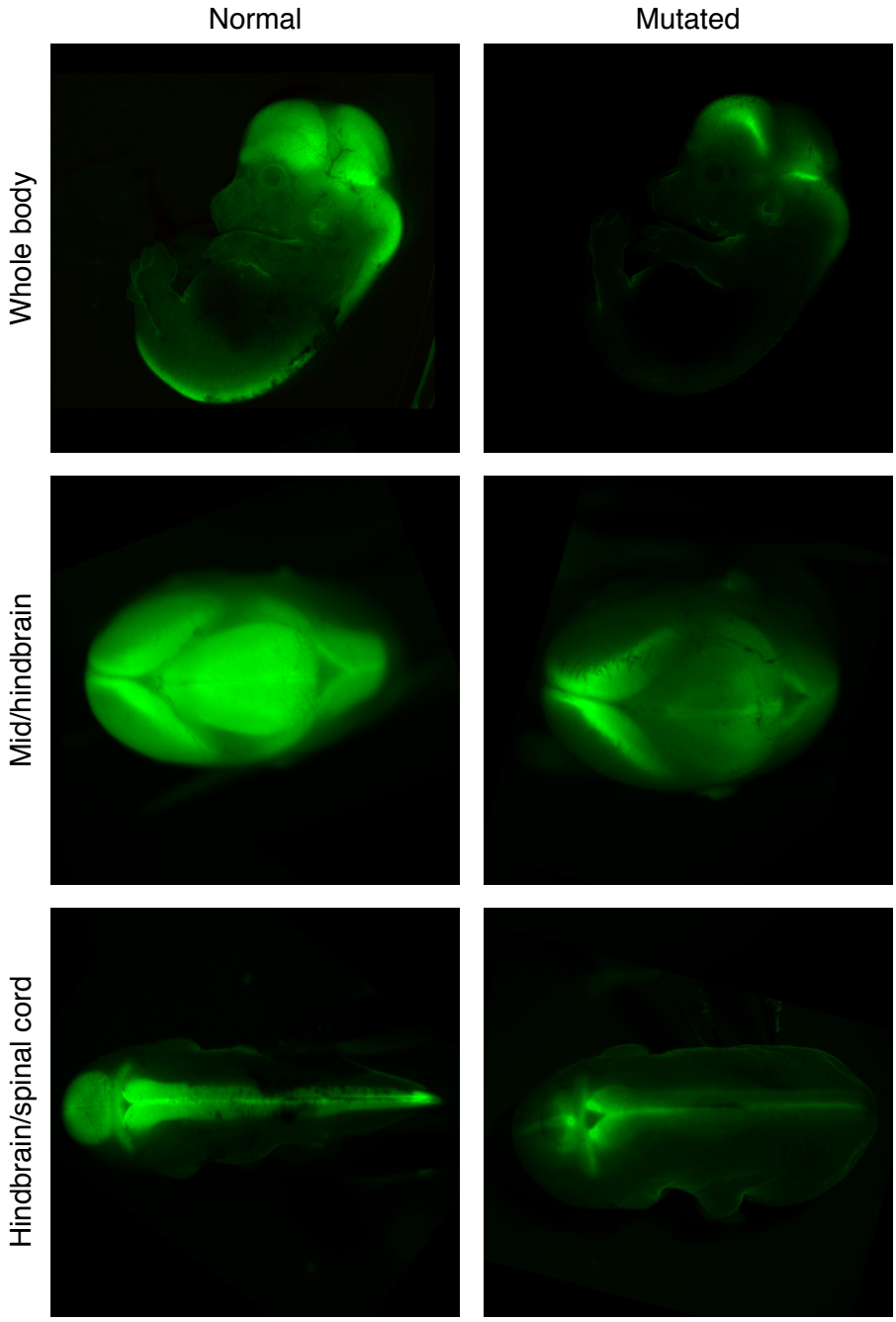

Fig. S3. 23-kb upstream region of human *GPR56* drives GFP reporter expression in the central nervous system in the developing mouse embryos. The forebrain, midbrain, hindbrain, and spinal cord express GFP under the normal promoter. The 15-bp deletion ablates gene expression in the lateral neocortex and decreases the midbrain, hindbrain, and spinal cord expression.

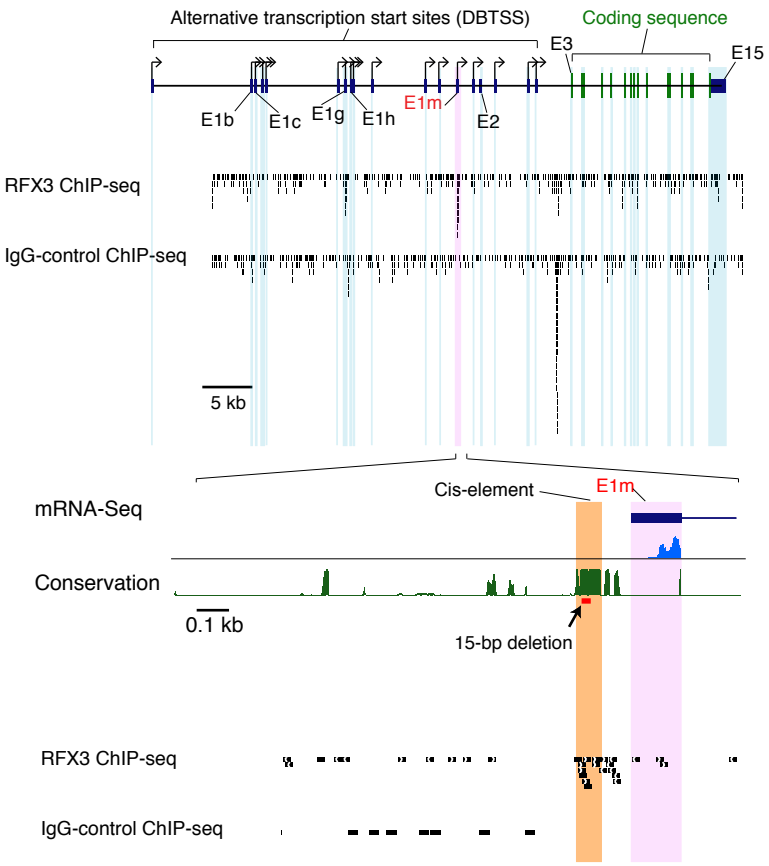

Fig. S4. ChIP-Seq data reveal RFX3 binding to the cis-regulatory element upstream of human *GPR56* e1m.

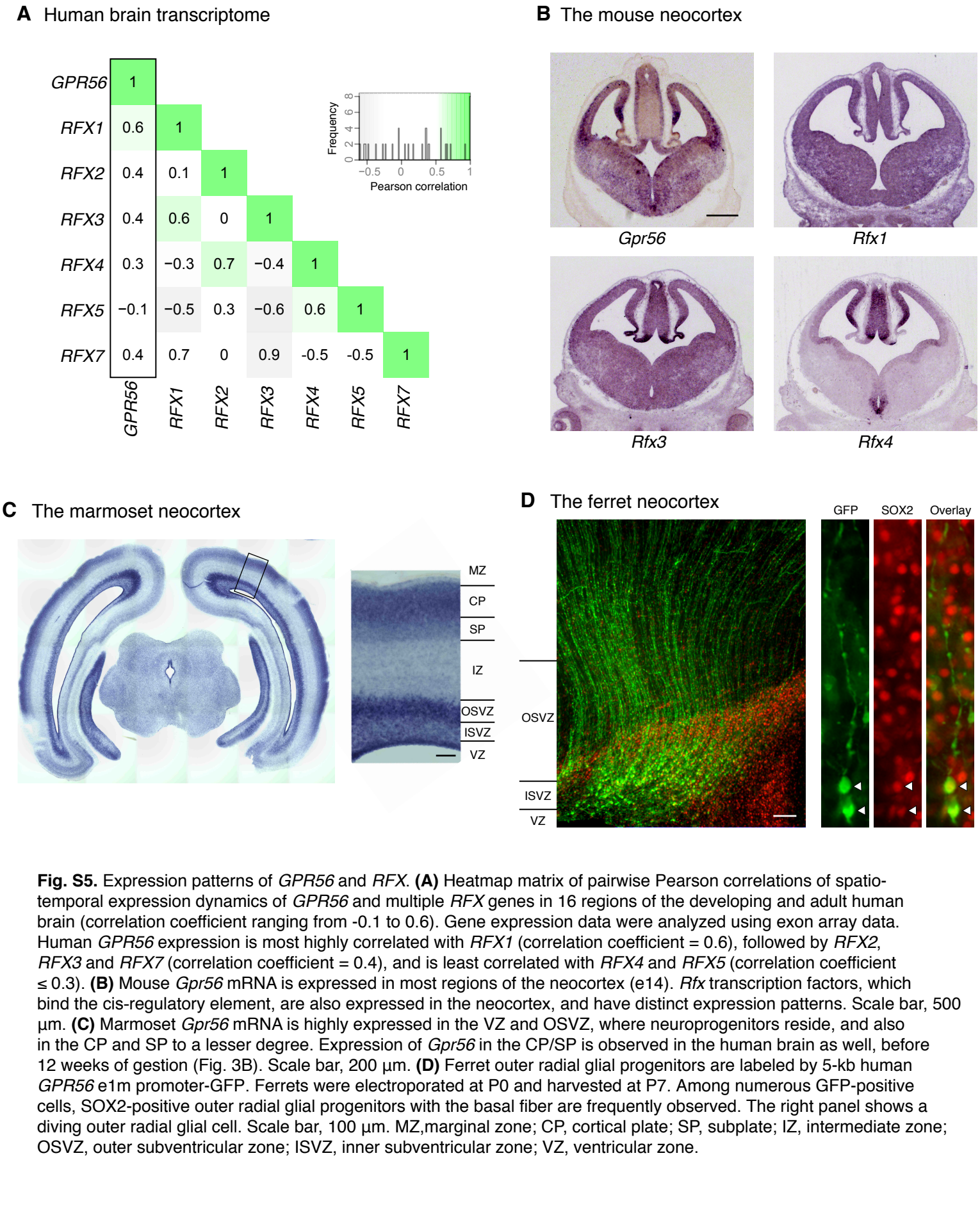

Fig. S5. Expression patterns of *GPR56* and *RFX*. **(A)** Heatmap matrix of pairwise Pearson correlations of spatio-temporal expression dynamics of *GPR56* and multiple *RFX* genes in 16 regions of the developing and adult human brain (correlation coefficient ranging from -0.1 to 0.6). Gene expression data were analyzed using exon array data. Human *GPR56* expression is most highly correlated with *RFX1* (correlation coefficient = 0.6), followed by *RFX2*, *RFX3* and *RFX7* (correlation coefficient = 0.4), and is least correlated with *RFX4* and *RFX5* (correlation coefficient ≤ 0.3). **(B)** Mouse *Gpr56* mRNA is expressed in most regions of the neocortex (e14). *Rfx* transcription factors, which bind the cis-regulatory element, are also expressed in the neocortex, and have distinct expression patterns. Scale bar, 500 µm. **(C)** Marmoset *Gpr56* mRNA is highly expressed in the VZ and OSVZ, where neuroprogenitors reside, and also in the CP and SP to a lesser degree. Expression of *Gpr56* in the CP/SP is observed in the human brain as well, before 12 weeks of gestion (Fig. 3B). Scale bar, 200 µm. **(D)** Ferret outer radial glial progenitors are labeled by 5-kb human *GPR56* e1m promoter-GFP. Ferrets were electroporated at P0 and harvested at P7. Among numerous GFP-positive cells, SOX2-positive outer radial glial progenitors with the basal fiber are frequently observed. The right panel shows a diving outer radial glial cell. Scale bar, 100 µm. MZ,marginal zone; CP, cortical plate; SP, subplate; IZ, intermediate zone; OSVZ, outer subventricular zone; ISVZ, inner subventricular zone; VZ, ventricular zone.

A

```
Human      CCCCATAAATCGCTGTCC------TAACCCCTGCCCTCCCTCCTGCCAGCTCCCTGTCTGG---CCTGGGCAGCGTCTGAGTTGAGG-------ACTTGGGAACAG
Marmoset   CCCGATAAGTCACCATCC------TAAGCCCTGTCCTCCCTCCTGCCAGCTGCCTATCTGG---CCTGGGCAGCGTCTGAGTTGAGG-------TCTTGGGCACAG
Dolphin    CCCCATAATCTGGTGTCC------TAAACTCTGCCTTTCTTCCTGCCAGCTCCCTA--------CCTGGCCAGCATCCAAGTAAGGG------GACTTGGGCACAG
Cat        CTCTATAA----------------------------CCTCCTCCCGCCAGCTCTCCCTGCTGGACCCAGGGCAGCATCTGAGTCTGGA------GACTTGGGTACCA
Mouse      --CTAGGACCCGTTCTCTCGAGTGTGAACCCAG--CTTGTCCCTGCTAGTAACCTGCTTTAGC-CCCAGGCAGCCTCAGGACGAAAGCTCTCACGCTTGGGTACA-
             * *  *                              ** ** **    *         **  * **** **                    ****** **

Human      GACAAGTTACGGAGCCACGTTGCTTTGCTGGGTCTGAGCCGGGGTGTGACGTAG-----TCCCTGCAGCTGCCAACGGTTGCCAGGGCAACGGTTGCCAGGGGCTG
Marmoset   GACAAGTTACGGAGCCACATTGCTTTGCTGGGTCTGAGCCGAGCTGTGACGTAG-----TCCCTGCAGCTGCCAACAGTTGCCAGGGCAACGGTTGCTAGGGGCTG
Dolphin    GACAAGTCA--GGGC--CTGCGCTGTGCTGGGTTGGAGCTGGGCAGTGACGTAG-----TCCCTGCAGCTGCCAACGGTTGCCAGGGCAACGGTTGCCAGGGGCTG
Cat        GACAAGTTAGGGGGC--TTGTGCTGTGCTGGGTCGGAGCCGGG-AGTGACGTATTTGCCTTTCTGCAGCTGCCAACGGTTGCCAGGGAAACGGTTGCCAGGGGCTG
Mouse      GACAAGTTGGAGAGC--CCGCGCTGT----------AAGCCAGGCAGTGACGCAG-----TCCATGCAGCTGCCAACGGTTGCCAGGGGAACGGTTGCCAGGGGCTG
           *******    * **      *** *          ***   *  ****** *      *   ************ ********** ********* *********

Human      CTGTCACCTGCGCCCCTTCTCC-------------CGCGCTGGCGGCTGGGGCTTCTCAGCCTCTATTCCCTGGCTGTCCCCTTTGTTTGAAGCTCCAGTGAGGGA
Marmoset   CTGTCACCTGCGCCCCTTCTCT-------------GGAGCTGGCGGCTGCGGCTTCTCAGCC--TCTTCCCTGGCTGTCCCCTTTGTTTGGAGCTCCAGTGAGGGA
Dolphin    CTGTCACCTGCGCCCCTTTTCC-------------CGGGTTGGCGGCTGGGACTT-GCAGCCCGTCTTCCCAGGCTGCCCGCTTTGTTTGAGGCTCCGGTGAGGGG
Cat        CTGTCACCTGCGCCCCTTCTCCCCCCCCCCCCCCCACCGGCCGGTGACTGGGGCTT-GCAGCCCGTCTTCCCTGGCTGCCCGCTTTGTTTGAAGCTCCAGGGAGGGG
Mouse      CTGTCACCTGCGCCCCTTCCTCCCCCTT-------GGCGCTGGAGGCCCGGGCTTCTCAGCTCAGCTTCCC-GCCTGCCCCCTTTGTTTGAAGCCCTAGTAAGGGG
           ******************                  *  ** * *   * ***  ****     ***** * *** ** *********  ** *  *  ****

Human      G-------CAGTGGCTGGGGTGG-------------CCCAGCTTCAAAGT
Marmoset   G-------CAGTGGCTGGGGTAG-------------CCCAGCTTCAAAGT
Dolphin    GGCGGGGACCGAGGCTGGGGAGG-------------CTCAGCTTCAAAGT
Cat        G-------CAGGGGCTGGGGTGG-------------CTCTGCTTGGAAAT
Mouse      A-------TGGTGACTGGGGGGGGGGGTAAGGGGGACCCAGGCTTTCATT
                 * * ******  *             * * *  *   * *
```

B

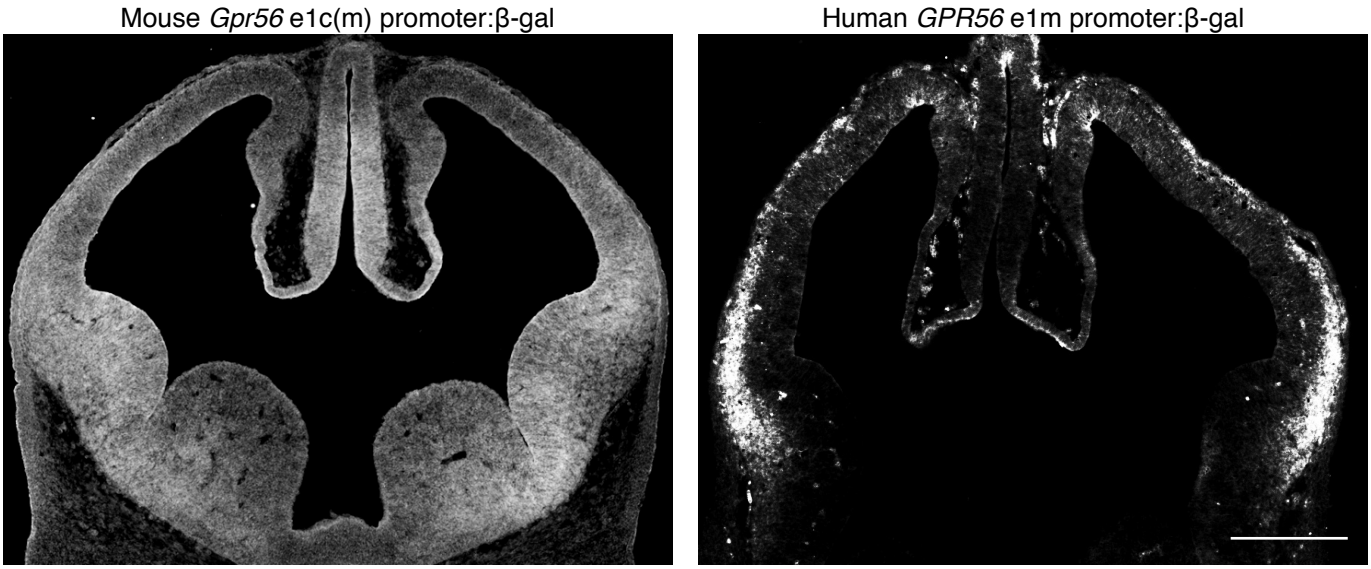

Fig. S6. *GPR56* e1m promoters from different species. **(A)** These promoters were used for mouse transgenesis. Bioinformatics predicts that the cis-regulatory element harbors an RFX binding motif, which is abolished upon the 15-bp deletion. The cis-regulatory element is underlined, the RFX binding motif is highlighted in yellow, and the two 15-bp repeats are demarcated with red rectangles. The underlined sequence is 100% conserved between humans and other anthropoids, old-world monkeys, and dolphins, and 98% conserved between humans and mice. The two copies of 15 bp are identical in human and dolphin, but not in marmoset, cat, and mouse. Human e1m promoter has multiple transcription start sites, and the most favored one is demarcated with a red arrow.
(B) Immunohistochemistry of β-gal shows that 300-bp human e1m promoter drives expression mostly in non-ventricular zone, whereas the mouse homolog drives in all layers (E13.5). Scale bar, 500 μm.

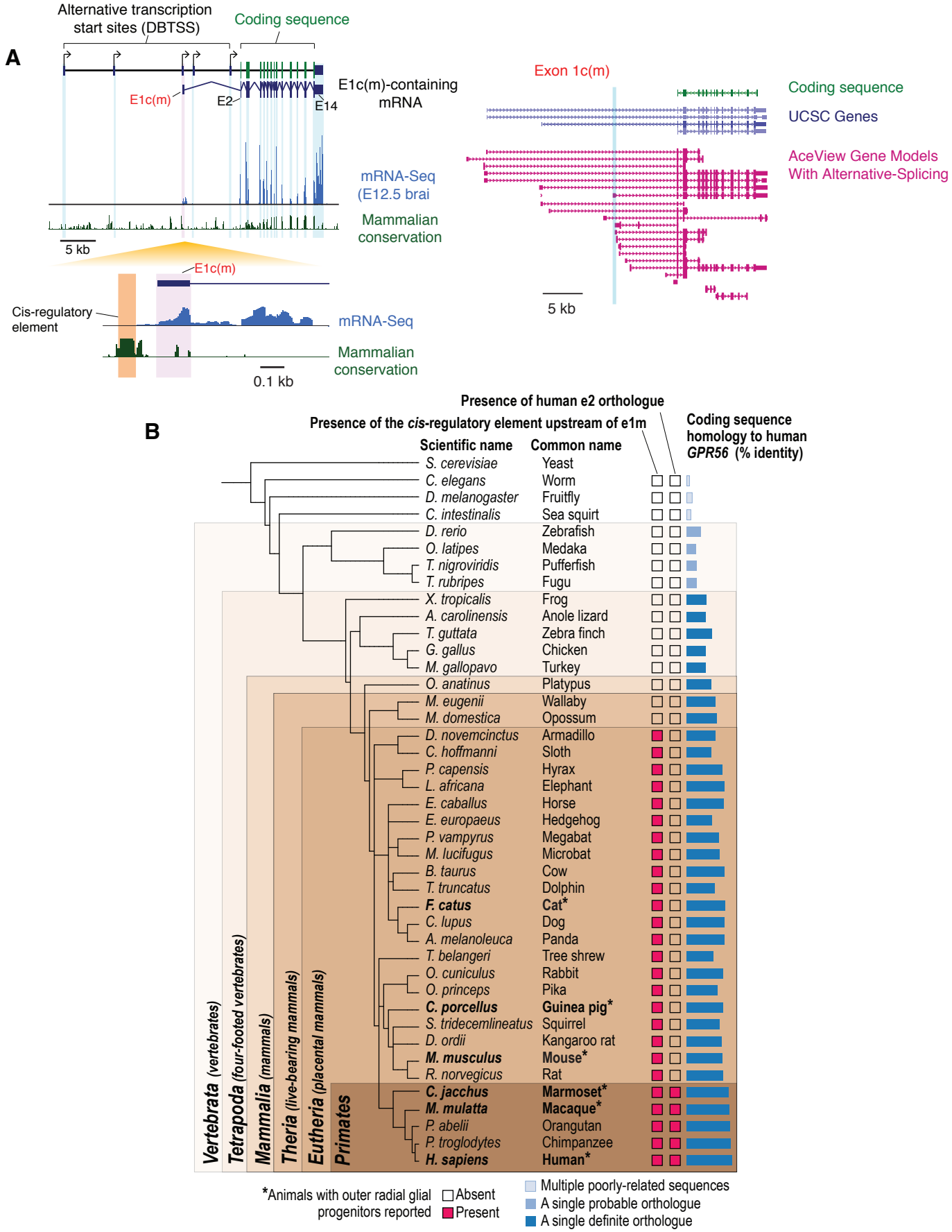

Fig. S7. Genomic organization of mouse *Gpr56* and evolution of the *GPR56* gene. **(A)** Mouse *Gpr56* has 5 alternative transcription start sites (left) and about 20 alternative splice variants (right), according to DBTSS and the AceView database. Regardless, e1c(m), which corresponds to human e1m, is still the most robustly transcribed first exon (mRNA-Seq track). **(B)** The protein-coding sequence of *GPR56* arose in Vertebrata, while e1m's cis-regulatory element is distinct to placental mammals and e2 is distinct to primates.

Identification			Clinical Features				Radiological Features	
Diagnosis	Individual	Origin/Pedigree	Cognitive development	Motor development	Epilepsy	Other clinical signs	Extent of polymicrogyria	Other radiological signs
"Classical" BFPP (Bilateral Frontal Parietal polymicrogyria)	Refer to Piao, *et al*. (2004) and Chang, *et al*. (2003).		Moderate to severe intellectual disability	Most commonly spastic quadriparesis form of cerebral palsy	Medically refractory generalized seizures	Cerebellar dysfunction, dysconjugate gaze	Bilateral frontal and parietal lobes, with a decreasing anterior-posterior gradient	Patchy bilateral white matter signal abnormalities, brainstem and/or cerebellar hypoplasia
Perisylvian polymicrogyria	Pedigree 1, Individual V:1	Turkey; Parents are first cousins once removed	Intellectual disability (IQ 48), mild delay, can read and write	No reported abnormalities	Medically refractory seizures	Left eye esotropia, nystagmus, mild bilateral thenar atrophy,	Lateral frontal and temporal lobes bilaterally, sparing inferomedial lobes and poles	
Perisylvian polymicrogyria	Pedigree 1, Individual V:2	Turkey; Parents are first cousins once removed	Intellectual disability (IQ 57), special education, cannot read	No reported abnormalities	Medically refractory seizures	Obesity	Lateral frontal and temporal lobes bilaterally, sparing inferomedial lobes and poles	
Perisylvian polymicrogyria	Pedigree 2 Individual VI:1	Irish American; Parents are third cousins	Special education in math, completed regular school, inattention and some frontal executive dysfunction	No reported abnormalities	Febrile seizures, nocturnal seizures with tonic stiffening and vocalization	Right eye exotropia	Lateral frontal and temporal lobes and perisylvian regions, sparing medial lobes	One or two isolated hyper-intense lesions on FLAIR, no widespread abnormality
Perisylvian polymicrogyria	Pedigree 2 Individual VI:2	Irish American; Parents are third cousins	Odd component and manner of behaving similar to the sibling (pedigree 2, VI:1)	No reported abnormalities	Febrile nocturnal seizures		Frontal lobes, particularly over the dorsolateral and suprasylvian regions bilaterally. Temporal lobes mildly affected.	Many bilateral frontal prominent perivascular spaces, particularly on right (CSF-intensity on FLAIR)
Perisylvian polymicrogyria	Pedigree 3, Individual II:1	Irish American	No reported abnormalities	No reported abnormalities	Generalized convulsions with tonic stiffening and vocalization		Lateral frontal lobes and supraperisylvian regions, sparing medial lobes	Some prominent bilateral frontal perivascular spaces

Table S1. Clinical and radiological features of individuals with perisylvian polymicrogyria and BFPP.

Non-exonic element #	Position	Size (nt)
1	chr16:56169282-56169345	63
2	chr16:56170515-56170705	192
3	chr16:56182955-56183014	57
4	chr16:56188549-56188635	86
5	chr16:56193254-56193339	86
6	chr16:56194448-56195228	779
7	chr16:56195485-56195715	230
8	chr16:56195997-56196097	100
9	chr16:56196255-56197163	908
10	chr16:56198627-56198661	34
11	chr16:56208995-56209040	45
12	chr16:56209170-56209229	60
13	chr16:56211401-56211510	108
14	chr16:56212494-56212711	217
15	chr16:56214031-56214357	326
16	chr16:56215091-56215417	326
17	chr16:56219296-56219367	72
18	chr16:56219558-56219655	97
19	chr16:56219826-56220020	194
20	chr16:56221668-56221797	129
21	chr16:56222802-56222841	38
22	chr16:56223082-56223140	58
23	chr16:56223252-56223291	38
24	chr16:56224140-56224177	38
25	chr16:56225658-56225744	86
26	chr16:56228983-56229243	260
27	chr16:56229918-56229956	38
28	**chr16:56230736-56230911**	**175**
29	chr16:56232380-56232439	58
30	chr16:56233720-56233783	64
31	chr16:56235022-56235166	144
32	chr16:56237556-56237698	142
33	chr16:56238700-56238763	62
34	chr16:56240581-56240650	70
35	chr16:56243150-56243219	69
36	chr16:56251627-56251696	69
37	chr16:56253454-56253505	51
38	chr16:56257690-56257741	51

Table S2. Sequenced non-exonic elements of *GPR56*. Element #28 contains e1m's *cis*-regulatory element, in which the 15-bp is deleted. (NCBI36/hg18 assembly).

Movie S1

MRI of the entire brain of a control subject, from back to front.

Movie S2

MRI of the entire brain of an individual with perisylvian polymicrogyria, from back to front.

References

1. P. Rakic, Evolution of the neocortex: A perspective from developmental biology. *Nat. Rev. Neurosci.* **10**, 724–735 (2009). doi:10.1038/nrn2719 Medline

2. J. H. Lui, D. V. Hansen, A. R. Kriegstein, Development and evolution of the human neocortex. *Cell* **146**, 18–36 (2011). doi:10.1016/j.cell.2011.06.030 Medline

3. K. Zilles, N. Palomero-Gallagher, K. Amunts, Development of cortical folding during evolution and ontogeny. *Trends Neurosci.* **36**, 275–284 (2013). doi:10.1016/j.tins.2013.01.006 Medline

4. K. Amunts, M. Lenzen, A. D. Friederici, A. Schleicher, P. Morosan, N. Palomero-Gallagher, K. Zilles, Broca's region: Novel organizational principles and multiple receptor mapping. *PLOS Biol.* **8**, e1000489 (2010). doi:10.1371/journal.pbio.1000489 Medline

5. J. A. Golden, B. N. Harding, Cortical malformations: Unfolding polymicrogyria. *Nat. Rev. Neurol* **6**, 471–472 (2010). doi:10.1038/nrneurol.2010.118 Medline

6. A. J. Barkovich, Current concepts of polymicrogyria. *Neuroradiology* **52**, 479–487 (2010). doi:10.1007/s00234-009-0644-2 Medline

7. X. Piao, R. S. Hill, A. Bodell, B. S. Chang, L. Basel-Vanagaite, R. Straussberg, W. B. Dobyns, B. Qasrawi, R. M. Winter, A. M. Innes, T. Voit, M. E. Ross, J. L. Michaud, J. C. Déscarie, A. J. Barkovich, C. A. Walsh, G protein–coupled receptor-dependent development of human frontal cortex. *Science* **303**, 2033–2036 (2004). doi:10.1126/science.1092780 Medline

8. X. Piao, B. S. Chang, A. Bodell, K. Woods, B. Benzeev, M. Topcu, R. Guerrini, H. Goldberg-Stern, L. Sztriha, W. B. Dobyns, A. J. Barkovich, C. A. Walsh, Genotype-phenotype analysis of human frontoparietal polymicrogyria syndromes. *Ann. Neurol.* **58**, 680–687 (2005). doi:10.1002/ana.20616 Medline

9. N. Bahi-Buisson, K. Poirier, N. Boddaert, C. Fallet-Bianco, N. Specchio, E. Bertini, O. Caglayan, K. Lascelles, C. Elie, J. Rambaud, M. Baulac, I. An, P. Dias, V. des Portes, M. L. Moutard, C. Soufflet, M. El Maleh, C. Beldjord, L. Villard, J. Chelly, GPR56-related bilateral frontoparietal polymicrogyria: Further evidence for an overlap with the cobblestone complex. *Brain* **133**, 3194–3209 (2010). doi:10.1093/brain/awq259 Medline

10. D. Thierry-Mieg, J. Thierry-Mieg, AceView: A comprehensive cDNA-supported gene and transcripts annotation. *Genome Biol.* **7** (suppl. 1), S12–S14 (2006). doi:10.1186/gb-2006-7-s1-s12 Medline

11. Y. Suzuki, R. Yamashita, K. Nakai, S. Sugano, DBTSS: DataBase of human Transcriptional Start Sites and full-length cDNAs. *Nucleic Acids Res.* **30**, 328–331 (2002). doi:10.1093/nar/30.1.328 Medline

12. S. J. Ansley, J. L. Badano, O. E. Blacque, J. Hill, B. E. Hoskins, C. C. Leitch, J. C. Kim, A. J. Ross, E. R. Eichers, T. M. Teslovich, A. K. Mah, R. C. Johnsen, J. C. Cavender, R. A. Lewis, M. R. Leroux, P. L. Beales, N. Katsanis, Basal body

dysfunction is a likely cause of pleiotropic Bardet-Biedl syndrome. *Nature* **425**, 628–633 (2003). doi:10.1038/nature02030 Medline

13. A. Jolma, T. Kivioja, J. Toivonen, L. Cheng, G. Wei, M. Enge, M. Taipale, J. M. Vaquerizas, J. Yan, M. J. Sillanpää, M. Bonke, K. Palin, S. Talukder, T. R. Hughes, N. M. Luscombe, E. Ukkonen, J. Taipale, Multiplexed massively parallel SELEX for characterization of human transcription factor binding specificities. *Genome Res.* **20**, 861–873 (2010). doi:10.1101/gr.100552.109 Medline

14. D. Zhang, D. J. Stumpo, J. P. Graves, L. M. DeGraff, S. F. Grissom, J. B. Collins, L. Li, D. C. Zeldin, P. J. Blackshear, Identification of potential target genes for RFX4_v3, a transcription factor critical for brain development. *J. Neurochem.* **98**, 860–875 (2006). doi:10.1111/j.1471-4159.2006.03930.x Medline

15. H. J. Kang, Y. I. Kawasawa, F. Cheng, Y. Zhu, X. Xu, M. Li, A. M. Sousa, M. Pletikos, K. A. Meyer, G. Sedmak, T. Guennel, Y. Shin, M. B. Johnson, Z. Krsnik, S. Mayer, S. Fertuzinhos, S. Umlauf, S. N. Lisgo, A. Vortmeyer, D. R. Weinberger, S. Mane, T. M. Hyde, A. Huttner, M. Reimers, J. E. Kleinman, N. Sestan, Spatio-temporal transcriptome of the human brain. *Nature* **478**, 483–489 (2011). doi:10.1038/nature10523 Medline

16. S. Li, Z. Jin, S. Koirala, L. Bu, L. Xu, R. O. Hynes, C. A. Walsh, G. Corfas, X. Piao, GPR56 regulates pial basement membrane integrity and cortical lamination. *J. Neurosci.* **28**, 5817–5826 (2008). doi:10.1523/JNEUROSCI.0853-08.2008 Medline

17. R. Luo, S. J. Jeong, Z. Jin, N. Strokes, S. Li, X. Piao, G protein-coupled receptor 56 and collagen III, a receptor-ligand pair, regulates cortical development and lamination. *Proc. Natl. Acad. Sci. U.S.A.* **108**, 12925–12930 (2011). doi:10.1073/pnas.1104821108 Medline

18. S. J. Jeong, R. Luo, S. Li, N. Strokes, X. Piao, Characterization of G protein-coupled receptor 56 protein expression in the mouse developing neocortex. *J. Comp. Neurol.* **520**, 2930–2940 (2012). doi:10.1002/cne.23076 Medline

19. L. Baala, S. Briault, H. C. Etchevers, F. Laumonnier, A. Natiq, J. Amiel, N. Boddaert, C. Picard, A. Sbiti, A. Asermouh, T. Attié-Bitach, F. Encha-Razavi, A. Munnich, A. Sefiani, S. Lyonnet, Homozygous silencing of T-box transcription factor EOMES leads to microcephaly with polymicrogyria and corpus callosum agenesis. *Nat. Genet.* **39**, 454–456 (2007). doi:10.1038/ng1993 Medline

20. T. S. Mikkelsen, M. J. Wakefield, B. Aken, C. T. Amemiya, J. L. Chang, S. Duke, M. Garber, A. J. Gentles, L. Goodstadt, A. Heger, J. Jurka, M. Kamal, E. Mauceli, S. M. J. Searle, T. Sharpe, M. L. Baker, M. A. Batzer, P. V. Benos, K. Belov, M. Clamp, A. Cook, J. Cuff, R. Das, L. Davidow, J. E. Deakin, M. J. Fazzari, J. L. Glass, M. Grabherr, J. M. Greally, W. Gu, T. A. Hore, G. A. Huttley, M. Kleber, R. L. Jirtle, E. Koina, J. T. Lee, S. Mahony, M. A. Marra, R. D. Miller, R. D. Nicholls, M. Oda, A. T. Papenfuss, Z. E. Parra, D. D. Pollock, D. A. Ray, J. E. Schein, T. P. Speed, K. Thompson, J. L. VandeBerg, C. M. Wade, J. A. Walker, P. D. Waters, C. Webber, J. R. Weidman, X. Xie, M. C. Zody, J. A. Graves, C. P. Ponting, M. Breen, P. B. Samollow, E. S. Lander, K. Lindblad-Toh; Broad

Institute Genome Sequencing Platform, Broad Institute Whole Genome Assembly Team, Genome of the marsupial *Monodelphis domestica* reveals innovation in non-coding sequences. *Nature* **447**, 167–177 (2007). doi:10.1038/nature05805 Medline

21. L. Xu, R. O. Hynes, GPR56 and TG2: Possible roles in suppression of tumor growth by the microenvironment. *Cell Cycle* **6**, 160–165 (2007). doi:10.4161/cc.6.2.3760 Medline

22. R. Radakovits, C. S. Barros, R. Belvindrah, B. Patton, U. Müller, Regulation of radial glial survival by signals from the meninges. *J. Neurosci.* **29**, 7694–7705 (2009). doi:10.1523/JNEUROSCI.5537-08.2009 Medline

23. S. A. Fietz, I. Kelava, J. Vogt, M. Wilsch-Bräuninger, D. Stenzel, J. L. Fish, D. Corbeil, A. Riehn, W. Distler, R. Nitsch, W. B. Huttner, OSVZ progenitors of human and ferret neocortex are epithelial-like and expand by integrin signaling. *Nat. Neurosci.* **13**, 690–699 (2010). doi:10.1038/nn.2553 Medline

24. S. J. Jeong, R. Luo, K. Singer, S. Giera, J. Kreidberg, D. Kiyozumi, C. Shimono, K. Sekiguchi, X. Piao, GPR56 functions together with α3β1 integrin in regulating cerebral cortical development. *PLOS ONE* **8**, e68781 (2013). doi:10.1371/journal.pone.0068781 Medline

25. R. Guerrini, A. J. Barkovich, L. Sztriha, W. B. Dobyns, Bilateral frontal polymicrogyria: A newly recognized brain malformation syndrome. *Neurology* **54**, 909–913 (2000). doi:10.1212/WNL.54.4.909 Medline

26. B. S. Chang, X. Piao, A. Bodell, L. Basel-Vanagaite, R. Straussberg, W. B. Dobyns, B. Qasrawi, R. M. Winter, A. M. Innes, T. Voit, P. E. Grant, A. J. Barkovich, C. A. Walsh, Bilateral frontoparietal polymicrogyria: Clinical and radiological features in 10 families with linkage to chromosome 16. *Ann. Neurol.* **53**, 596–606 (2003). doi:10.1002/ana.10520 Medline

27. D. F. Gudbjartsson, K. Jonasson, M. L. Frigge, A. Kong, Allegro, a new computer program for multipoint linkage analysis. *Nat. Genet.* **25**, 12–13 (2000). doi:10.1038/75514 Medline

28. A. M. Dale, B. Fischl, M. I. Sereno, Cortical surface-based analysis. I. Segmentation and surface reconstruction. *Neuroimage* **9**, 179–194 (1999). doi:10.1006/nimg.1998.0395 Medline

29. K. Im, R. Pienaar, J. M. Lee, J. K. Seong, Y. Y. Choi, K. H. Lee, P. E. Grant, Quantitative comparison and analysis of sulcal patterns using sulcal graph matching: A twin study. *Neuroimage* **57**, 1077–1086 (2011). doi:10.1016/j.neuroimage.2011.04.062 Medline

30. W. J. Kent, C. W. Sugnet, T. S. Furey, K. M. Roskin, T. H. Pringle, A. M. Zahler, D. Haussler, The human genome browser at UCSC. *Genome Res.* **12**, 996–1006 (2002). Medline

31. S. Warming, N. Costantino, D. L. Court, N. A. Jenkins, N. G. Copeland, Simple and highly efficient BAC recombineering using galK selection. *Nucleic Acids Res.* **33**, e36 (2005). doi:10.1093/nar/gni035 Medline

32. B. C. Bjork, Y. Fujiwara, S. W. Davis, H. Qiu, T. L. Saunders, P. Sandy, S. Orkin, S. A. Camper, D. R. Beier, A transient transgenic RNAi strategy for rapid characterization of gene function during embryonic development. *PLOS ONE* **5**, e14375 (2010). doi:10.1371/journal.pone.0014375 Medline

33. Y. J. Yang, A. E. Baltus, R. S. Mathew, E. A. Murphy, G. D. Evrony, D. M. Gonzalez, E. P. Wang, C. A. Marshall-Walker, B. J. Barry, J. Murn, A. Tatarakis, M. A. Mahajan, H. H. Samuels, Y. Shi, J. A. Golden, M. Mahajnah, R. Shenhav, C. A. Walsh, Microcephaly gene links trithorax and REST/NRSF to control neural stem cell proliferation and differentiation. *Cell* **151**, 1097–1112 (2012). doi:10.1016/j.cell.2012.10.043 Medline

34. P. A. Gray, H. Fu, P. Luo, Q. Zhao, J. Yu, A. Ferrari, T. Tenzen, D. I. Yuk, E. F. Tsung, Z. Cai, J. A. Alberta, L. P. Cheng, Y. Liu, J. M. Stenman, M. T. Valerius, N. Billings, H. A. Kim, M. E. Greenberg, A. P. McMahon, D. H. Rowitch, C. D. Stiles, Q. Ma, Mouse brain organization revealed through direct genome-scale TF expression analysis. *Science* **306**, 2255–2257 (2004). doi:10.1126/science.1104935 Medline

35. N. Bayatti, S. Sarma, C. Shaw, J. A. Eyre, D. A. Vouyiouklis, S. Lindsay, G. J. Clowry, Progressive loss of PAX6, TBR2, NEUROD and TBR1 mRNA gradients correlates with translocation of EMX2 to the cortical plate during human cortical development. *Eur. J. Neurosci.* **28**, 1449–1456 (2008). doi:10.1111/j.1460-9568.2008.06475.x Medline

36. H. Mashiko, A. C. Yoshida, S. S. Kikuchi, K. Niimi, E. Takahashi, J. Aruga, H. Okano, T. Shimogori, Comparative anatomy of marmoset and mouse cortex from genomic expression. *J. Neurosci.* **32**, 5039–5053 (2012). doi:10.1523/JNEUROSCI.4788-11.2012 Medline

37. S. Maijgren, I. Sur, M. Nilsson, R. Toftgård, Involvement of RFX proteins in transcriptional activation from a Ras-responsive enhancer element. *Arch. Dermatol. Res.* **295**, 482–489 (2004). doi:10.1007/s00403-004-0456-5 Medline

38. M. B. Johnson, Y. I. Kawasawa, C. E. Mason, Z. Krsnik, G. Coppola, D. Bogdanović, D. H. Geschwind, S. M. Mane, M. W. State, N. Sestan, Functional and evolutionary insights into human brain development through global transcriptome analysis. *Neuron* **62**, 494–509 (2009). doi:10.1016/j.neuron.2009.03.027 Medline

39. B. Langmead, C. Trapnell, M. Pop, S. L. Salzberg, Ultrafast and memory-efficient alignment of short DNA sequences to the human genome. *Genome Biol.* **10**, R25 (2009). doi:10.1186/gb-2009-10-3-r25 Medline

40. I. Letunic, P. Bork, Interactive Tree Of Life v2: Online annotation and display of phylogenetic trees made easy. *Nucleic Acids Res.* **39**(suppl.), W475–W478 (2011). doi:10.1093/nar/gkr201 Medline